



HAL
open science

Segregation in InGaAs/GaAs Stranski-Krastanow layers grown by MOCVD

Emanuela Piscopiello, Andreas Rosenauer, Adriana Passaseo, Eduardo
Haroldo Montoya Rossi, Gustaaf van Tendeloo

► **To cite this version:**

Emanuela Piscopiello, Andreas Rosenauer, Adriana Passaseo, Eduardo Haroldo Montoya Rossi, Gustaaf van Tendeloo. Segregation in InGaAs/GaAs Stranski-Krastanow layers grown by MOCVD. *Philosophical Magazine*, 2005, 85 (32), pp.3857-3870. 10.1080/14786430500269402 . hal-00513590

HAL Id: hal-00513590

<https://hal.science/hal-00513590>

Submitted on 1 Sep 2010

HAL is a multi-disciplinary open access archive for the deposit and dissemination of scientific research documents, whether they are published or not. The documents may come from teaching and research institutions in France or abroad, or from public or private research centers.

L'archive ouverte pluridisciplinaire **HAL**, est destinée au dépôt et à la diffusion de documents scientifiques de niveau recherche, publiés ou non, émanant des établissements d'enseignement et de recherche français ou étrangers, des laboratoires publics ou privés.



Segregation in InGaAs/GaAs Stranski-Krastanow layers grown by MOCVD

Journal:	<i>Philosophical Magazine & Philosophical Magazine Letters</i>
Manuscript ID:	TPHM-05-Apr-0109.R1
Journal Selection:	Philosophical Magazine
Date Submitted by the Author:	02-Jul-2005
Complete List of Authors:	Piscopiello, Emanuela; ENEA-c.r. Brindisi, Materials and New Technologies Unit Composite and Nanostructured Materials Section; University of Antwerp, EMAT Rosenauer, Andreas; University Bremen, IFP Passaseo, Adriana; University of Lecce, NNL Haroldo Montoya Rossi, Eduardo; University of Antwerp, EMAT Van Tendeloo, Gustaaf; University of Antwerp, EMAT
Keywords:	quantum dots, image analysis, HRTEM, GaAs
Keywords (user supplied):	



1
2
3
4
5 **Segregation in InGaAs/GaAs Stranski-Krastanow layers grown**
6
7
8 **by Metal Organic Vapour Phase Epitaxy**
9

10
11
12
13 E. PISCOPIELLO et al.
14
15

16
17
18 Complete list of the authors:
19

20 **Dr. Emanuela Piscopiello**
21

22 EMAT, University of Antwerp,
23 Groenenborgerlaan 171, B-2020 Antwerp, Belgium
24

25 Present address:
26

27 ENEA - C.R. Brindisi
28 Materials and New Technologies Unit
29 Composite and Nanostructured Materials Section
30 S.S. 7 - Km 714
31 72100 Brindisi (Italy)
32
33 Tel: +39 0831 201518
34
35 e-mail: emanuela.piscopiello@brindisi.enea.it
36
37
38
39

40
41 **Prof. Dr. Andreas Rosenauer**
42

43 IFP - University Bremen
44 Otto-Hahn-Allee 1, 28359 Bremen, GERMANY
45
46 Tel: ++49 (0)421 218.8197
47
48 Fax: ++49 (0)421 218.7381
49
50 Email: rosenauer@ifp.uni-bremen.de
51
52

53 **Dr. Adriana Passaseo**
54

55 National Nanotechnology Laboratory,
56 INFN-Unita` di Lecce c/o Dipartimento di Ingegneria
57 dell'Innovazione, Universita` di Lecce,
58
59
60

1
2
3
4
5 Via Arnesano, 73100 Lecce, Italy

6 Tel: +39 832 298206

7
8 Fax: +39 832 298238

9
10 Email: adriana.passaseo@unile.it
11

12
13
14 Eduardo Haroldo Montoya Rossi

15
16 Instituto Peruano de Energía Nuclear,

17
18 Av. Canada 1470, Lima 41, Perú

19
20 c/o Prof. Dr. Gustaaf Van Tendeloo, EMAT; Univ. of Antwerp
21

22
23
24
25 Prof. Dr. Gustaaf Van Tendeloo

26
27 EMAT, University of Antwerp,

28
29 Groenenborgerlaan 171, B-2020 Antwerp, Belgium

30
31 tel. : +32-3-2653262,

32
33 fax : +32-3-2653257,

34
35 Email : staf.vantendeloo@ua.ac.be
36
37
38
39
40
41
42
43
44
45
46
47
48
49
50
51
52
53
54
55
56
57
58
59
60

Segregation in InGaAs/GaAs Stranski-Krastanow layers grown

by MOCVD

E. PISCOPIELLO¹, A. ROSENAUER^{1,2}, A. PASSASEO³, E. H. MONTOYA ROSSI⁴, and
G. VAN TENDELOO¹.

1. EMAT, University of Antwerp, Groenenborgerlaan 171, B-2020 Antwerp, Belgium

2. IFP - University Bremen, Otto-Hahn-Allee 1, 28359 Bremen, GERMANY

3. NNL, University of Lecce, via Arnesano, 73100 Lecce, Italy

4. Instituto Peruano de Energía Nuclear, Av. Canada 1470, Lima 41, Perú .

Abstract

Using quantitative high resolution transmission electron microscopy we studied the chemical morphology of wetting layers in InGaAs/GaAs quantum dot structures which were optimised for applications to optical devices operating around 1.3 μm . The samples are grown by low-pressure metal-organic chemical vapour deposition on GaAs substrates. Indium concentration profiles of the wetting layers are evaluated with the composition evaluation by the lattice fringe analysis method. The profiles reveal a clear signature of segregation. A fit of the profiles with the Muraki model for segregation (K. Muraki et al., Appl. Phys. Lett. **61** (1992), 557) reveals a segregation efficiency of $R=0.65\pm 0.05$ at the growth temperature of 550 °C, which is significantly lower than segregation efficiencies observed in samples grown by molecular beam epitaxy at similar temperatures.

Keywords: HRTEM, image analysis, quantum dots, GaAs

1. Introduction

Low-dimensional semiconductor materials have become one of the most active research fields in solid state physics, chemistry and engineering. Quantum well (QW) and quantum-dot (QD) structures produced by epitaxial growth techniques (mainly molecular beam epitaxy (MBE) and metalorganic chemical vapour deposition (MOCVD)) are of considerable technological interest, since they are used as active components in devices, e.g. in high-electron-mobility transistors and optoelectronics [1]. Especially the InGaAs/GaAs material system is being studied intensively because of the possibility to form self-organized QDs by means of the Stranski-Krastanow growth mode under certain conditions. The development of QD lasers is expected to lead to increased quantum efficiency and to lower the threshold current density [2]. Properties of optoelectronic devices depend on the chemical morphology of the QWs or QDs forming the active region of a device. The growth of semiconductor nanostructures is governed by a complex and not fully understood interplay of surface and interface energies, formation of strain energy, elastic or plastic relaxation of strain energy, as well as by the kinetic growth processes such as adatom migration, interdiffusion and segregation.

Segregation is a known effect in MBE grown InGaAs/GaAs heterostructures [3,4] and leads to a strong enrichment of In on the growth surface compared to underlying completed mono layers (MLs). Moison et al. [5] attributed the effect to different chemical potentials of In and Ga atoms on the growth surface and suggested an exchange reaction of In and Ga in the topmost ("surface") layer and the underlying ("bulk") layer. The change of the free energy per atomic reaction was called the "segregation energy" E_S , and a value $E_S = 0.15$ eV was obtained [5] for InGaAs/GaAs at a growth temperature of 477 °C. Gerard [6] published a method to obtain the amount of In on the growth surface x_S by measuring a shift of the 2D-3D transition of InAs when grown on a predeposited layer of $\text{In}_{0.08}\text{Ga}_{0.92}\text{As}$. He found, that the amount of In on the surface of the predeposited layer with 8 % In was well described by the

1
2
3
4
5 segregation model of Moison [5] and obtained a segregation energy of $E_S = 0.17$ eV for a
6
7 growth temperature of 500 °C. For In-concentrations of the predeposited layer larger than 11
8
9 % he observed a strong deviation of x_S from the value predicted by the Moison model.
10
11 Toyoshima et al. [7] applied the method of Gerard to measure x_S for In-concentrations
12
13 between 15 % and 31 %. These authors found, that the amount of In x_S in the “In-floating
14
15 layer “ is well described by the phenomenological segregation model suggested by Muraki et
16
17 al. [8] also for nominal In-concentrations larger than 11 % where the Moison model failed.
18
19 Additionally, it was observed that the 2D-3D transition is correlated to the amount of In on
20
21 the growth surface and occurs when x_S reaches a value of more than 1.7 MLs. Rosenauer et
22
23 al. [9] measured In-concentration profiles of wetting layers in buried InAs/GaAs Stranski-
24
25 Krastanow structures by high-resolution transmission electron microscopy (HRTEM) and
26
27 found that the Muraki model [8] is in agreement with concentration profiles obtained. The
28
29 amount of In in the floating layer $x_S = 1.8$ MLs (1.5 MLs) was derived for growth temperatures
30
31 of 530 °C (480 °C) using a fit of the Muraki model to the experimental data. Evans et al. [10]
32
33 applied temperature-programmed desorption measurements and found that the steady-state In-
34
35 floating layer contains 1.3 ML (1.6 ML) In for a growth temperature of 480 °C (530 °C) and
36
37 that the surface-segregated In is liquid-like in character. Garcia et al. [11] found by in-situ
38
39 monitoring of stress acting on the GaAs substrate during the growth of InGaAs by MBE, that
40
41 the In-floating layer is not chemically bonded to the crystal surface. Further indication to the
42
43 mobile state of In atoms adsorbed in the In-floating layer has recently been given by RHEED
44
45 experiments carried out by Martini et al. [12]. The authors showed that the exponential
46
47 decrease of the RHEED oscillations observed at the onset of the InGaAs growth as well as the
48
49 increase of the signal during cap layer growth is caused by scattering of the electron beam by
50
51 mobile adatoms contained in the In-floating layer. Larive et al. [13] and Kaspi et al. [14]
52
53 observed an increase of the segregation with increasing growth temperature, which is in
54
55
56
57
58
59
60

1
2
3
4
5 contradiction to the Moison model [5]. Dehaese et al. [15] suggested a kinetic model
6
7 involving a two-energy level system which leads to the same segregation effect as the
8
9 Moison model for high growth temperatures larger than 500 °C, but additionally describes the
10 kinetic limitation of segregation at low temperature (400 °C). As shown by Gerard et al. [6],
11
12 this model is therefore also limited to In-concentrations below 11% for high growth
13
14 temperatures. Additionally, the exchange reaction of In and Ga between the surface and sub-
15
16 surface layer does not account for the liquid character of the In-atoms in the In-floating layer
17
18 evidenced recently [10,11,12], which limits x_s to values smaller or equal to 1 ML. Based on a
19
20 recent EFTEM study of Walther et al. [16], Cullis et al. [17] developed a segregation based
21
22 model for the critical thickness of the 2D-3D transition. In agreement with Toyoshima et al.
23
24 [7], the authors find that the 2D-3D transition occurs when the amount of In on the surface
25
26 exceeds a critical value. Applying the segregation model of Dehaese et al. [15] to InGaAs
27
28 layers with nominal In-concentrations of 25, 35 and 55 % at a growth temperature of 540 °C, a
29
30 critical value of $x_s=0.8-0.85$ MLs In was obtained.
31
32
33
34
35

36
37 During growth of a GaAs cap layer, the In-floating layer acts as a source for In atoms, leading
38
39 to a significant incorporation of In atoms into the cap layer. Thus, segregation leads to a
40
41 delayed incorporation of In atoms at the “lower” interface between the GaAs buffer and
42
43 InGaAs layer, and to an exponential decrease of the In-concentration within a GaAs cap layer
44
45 at the “upper” interface of the InGaAs layer.
46
47

48
49 Whereas segregation is intensively investigated for MBE grown structures, only little is
50
51 known about segregation during MOCVD growth. Evidence for segregation taking place in
52
53 atomic layer epitaxy using an MOCVD reactor was given by Arès et al. [18].
54

55
56 Here we present measurements of segregation efficiencies in MOCVD grown InGaAs/GaAs
57
58 using transmission electron microscopy (TEM) techniques. We evaluate In-concentration
59
60

1
2
3
4
5 profiles of the wetting layer (WL) of buried quantum dots and fit the results with the
6
7 segregation model of Muraki et al. [8].
8
9

10 11 12 **2. Experimental Set-Up**

13
14 The samples were grown in a horizontal low-pressure-MOCVD system (AIXTRON 200 AIX)
15
16 at 20 mbar with Trimethylgallium, Trimethylindium solution, and pure AsH₃ as source
17
18 materials; palladium purified H₂ with a flow rate of 7slm (standard litre per minute) was used
19
20 as a carrier gas. The growth was performed on (001) exactly oriented semi-insulating GaAs
21
22 substrates.
23
24

25
26 The investigated samples contain a 200 nm thick Si-doped GaAs buffer layer grown at a
27
28 temperature of 750°C, a 1- μ m Si-doped Al_{0.37}Ga_{0.63}As layer and a 80 nm GaAs layer,
29
30 followed by a 5 nm thick In_{0.10}Ga_{0.90}As layer, on top of which the deposition of the InGaAs
31
32 dots was carried out. The dots were covered with another 5 nm In_{0.10}Ga_{0.90}As and a 30 nm
33
34 thick GaAs cap layer. Two different samples were grown. In sample A, the thickness of the
35
36 InGaAs QD layer was 4 ML and the nominal In concentration $x_0=0.55$, whereas sample B
37
38 contains a 6 ML InGaAs QD layer with a nominal In concentration of $x_0=0.50$. During the
39
40 growth of the InGaAs layers, the growth temperature was fixed at 550 °C and the growth rate
41
42 at 1 ML/s. The AsH₃ partial pressure was kept at 1.4×10^{-1} mbar and 2.8×10^{-1} mbar for the
43
44 samples A and B, respectively. The In/Ga flow ratio was kept constant. During the capping
45
46 process the AsH₃ partial pressure was 5.7×10^{-1} mbar.
47
48
49

50
51 TEM samples were prepared by standard methods. Plan-view specimens were obtained by
52
53 grinding and polishing the substrate down to a thickness of about 20 μ m, followed by Ar ion
54
55 milling on the substrate side using an acceleration voltage of 4 kV and an incidence angle of
56
57 4°. Cross-section <001> and <110> TEM specimens were prepared by gluing two samples
58
59
60

1
2
3
4
5 face to face, cutting slices, dimple grinding and Ar ion milling. A JEOL 4000EX microscope
6
7 operating at 400kV with a Scherzer resolution of 0.17 nm was used.
8

9
10 Composition profiles of the wetting layers are obtained using the composition evaluation by
11 the lattice fringe analysis (CELFA) method [19,20]. (002) lattice fringe images are recorded
12 by tilting the specimen approximately 3° - 5° around an axis perpendicular to both the electron
13 beam direction and the interface plane. The excitation condition aimed at corresponds to a
14 center of the Laue circle (COLC) of (0,20,1.5) (a COLC of (0,20,2) would correspond to a
15 strongly excited (004) reflection) and was adjusted by selected-area diffraction in a region
16 including the investigated area or lying close it. The (002) beam is aligned parallel to the
17 optical axis and the objective aperture is set around the (002) and (000) reflections. The
18 CELFA method uses the following analysis steps: first, the image is subdivided into square
19 shaped image unit cells with a size corresponding to the 002 lattice plane spacing. For each
20 image unit cell n , the (signed) modulus $A_{002}(n)$ of the 002 Fourier component of the image
21 intensity is obtained by Fourier analysis. To account for variations of specimen thickness and
22 tilts [21,22,23] within the image, we use the following approach: Bloch wave calculations of
23 the modulus $A_{002}(x)$ of the 002 Fourier component of the image intensity as a function of the
24 In-concentration x were carried out for different thicknesses and tilts of the specimen [20].
25 These calculations showed, that the normalized modulus $A_{002}^N(x) = A_{002}(x)/A_{002}(x=0)$ only
26 weakly depends on specimen thickness and tilt. Therefore, we normalize the experimental
27 values $A_{002}(n)$ with respect to the GaAs region according to $A_{002}^N(n) = A_{002}(n)/A_{002}^0(n)$. Since
28 specimen thickness and tilt may vary within the image, an appropriate value $A_{002}^0(n)$ has to be
29 used for each image unit cell n . By using parts of the image lying in the regions of the GaAs
30 substrate or cap layer, a 2-dimensional third-order polynomial $A_{002}^0(n)$ is fitted to the values
31 $A_{002}(n)$. The experimentally obtained normalized modulus is then compared with values
32 calculated with the Bloch wave method. The Bloch wave calculations are based on the
33
34
35
36
37
38
39
40
41
42
43
44
45
46
47
48
49
50
51
52
53
54
55
56
57
58
59
60

1
2
3
4
5 knowledge of the Fourier components of the crystal potential. We compute the Fourier
6
7 components of the crystal potential by density functional theory methods [24]. This is done to
8
9 avoid the isolated atom approximation frequently used in TEM simulations. Additionally, the
10
11 effect of static displacements [24,25] occurring in ternary semiconductor material is also
12
13 taken into account.
14
15

21 3. Experimental Results

22
23 Fig. 1 shows plan view images from both samples A and B; the shape and size of the QDs are
24
25 clearly comparable. The density of the QDs is $2.3 \times 10^{10} \text{ cm}^{-2}$ for A and $7 \times 10^9 \text{ cm}^{-2}$ for B.
26
27 [Insert figure 1 about here]
28
29

30 Fig. 2 reproduces colour-coded maps of the In distribution in the $\text{In}_{1-x}\text{Ga}_x\text{As}$ WL evaluated
31
32 with the CELFA method. Although care was taken during the exposure of the images to use
33
34 regions where QDs were not visible, both images reveal small fluctuations of the In-
35
36 concentration within the InGaAs QW. Since these fluctuation do not only occur in the central
37
38 layer with high In concentration but also in the areas with nominally 10 % In, they are most
39
40 probably caused by surface roughness or contamination caused by ion milling during the
41
42 TEM specimen preparation, or by locally varying specimen tilt. Another possible origin could
43
44 be the presence of small dots or parts of already formed dots, depending on how the sample
45
46 was cut during the TEM cross-sectional specimen preparation. [Insert figure 2 about here]
47
48
49

50
51 Fig. 2 clearly evidences that the In-concentration in A is a few percent larger than in B, in
52
53 agreement with the values of the nominal concentration ($x_{0,A}=0.55$ and $x_{0,B}=0.50$).
54

55
56 For the quantification of the segregation efficiency, concentration profiles along the [001]
57
58 growth direction were obtained by averaging the evaluated In concentration along (002)
59
60

lattice planes. The results are shown in Fig. 3 for both samples A and B (open circles). The figures reveal a clear signature of segregation. [Insert figure 3 about here]

The In concentration rapidly increases at the two lower interfaces, whereas it decreases exponentially at the two upper interfaces close to the cap layer. For the evaluation of the segregation efficiency the measured profiles were fitted by the Muraki model. To model different local nominal In-concentrations ($x_0=0$ in the GaAs buffer and cap layers, $x_0 \approx 0.1$ in the $\text{In}_{0.10}\text{Ga}_{0.90}\text{As}$ layer and $x_0 = 0.55(0.5)$ in the QD layer in sample A(B)), we used the following iterative formulation of the Muraki model:

$$\begin{aligned}
 I \quad & x_b(n) = x_s(n) + x_0(n) \\
 II \quad & x_s(n+1) = x_b(n)R \quad , \\
 III \quad & x_b(n) = x_b(n)(1-R)
 \end{aligned}
 \tag{1}$$

where n is the number of the ML, R is the segregation efficiency, $x_b(n)$ is the In concentration in the upper crystal ML after growth of the n -th ML, and $x_s(n)$ is the In concentration in the In floating layer after growth of the n -th ML. In the literature (e.g. see ref. [7]), the amount of In in the floating layer is given in units of ML In, where 1 ML In corresponds to $x_s(n) = 1$. In the following, we shall use both notations. Equ. (1) comprises the following steps:

- I. After growth of ML ($n-1$) all In atoms of the In floating layer are incorporated into the upper crystal layer (corresponding to $x_b(n)$) and also the In atoms from the In source are added (corresponding to $x_0(n)$).
- II. Then, a fraction R of the In atoms in the upper crystal layer segregate to the new floating layer (corresponding to $x_s(n+1)$).
- III. The amount of Indium in the upper ML is decreased by the fraction of In atoms that segregated into the floating layer.

1
2
3
4
5 In Equ. (1), the segregation efficiency R as well as the position and thickness of the layers
6
7 were used as fitting parameters. The result of the fit is also shown in Fig. 3. The solid line
8
9 corresponds to the fitted concentration profile $x_b(n)$, and the dotted line indicates $x_0(n)$.
10
11 Obviously, the measured concentration profiles can well be fitted by the Muraki model,
12
13 clearly revealing that segregation is also present in samples grown by the MOCVD process.
14
15 From the fit of the Muraki model to our concentration profiles we found that the segregation
16
17 efficiency is $R=0.65\pm 0.05$ for both samples A and B. For the thickness of the central layer we
18
19 obtained 3 ML for sample A and 5 ML for sample B, compared to the nominal values of 4
20
21 ML and 6 ML, respectively.
22
23
24
25
26
27

28 **4. Discussion**

29
30 Although the fitted concentration profiles are generally in a fair agreement with the
31
32 experimental profiles, significant deviations are observed in both samples at the top of the
33
34 central InGaAs layer where the In concentration is large. In sample A(B), the measured In
35
36 concentration is approximately $\Delta x = 7\%$ (10%) below the value of the fitted profile. This
37
38 deviation can be explained by different effects.
39
40

41
42 First, it can be an artefact of the measurement of the In-concentration by the CELFA method.
43
44 If the specimen thickness assumed for the CELFA evaluation (30 nm) is wrong, the
45
46 evaluation contains errors that increase with increasing In-concentration. As the CELFA
47
48 technique uses a simple imaging condition where the relevant information (the local
49
50 composition) is almost solely transferred by only one reflection (the chemically sensitive 002
51
52 reflection) centred on the optical axis, objective lens defocus related artefacts are negligible in
53
54 a wide defocus range between approximately -150 and 50 nm [26].
55
56

57
58 Second, the InGaAs layers are strained. In a thin TEM specimen, compressively strained
59
60 layers are able to expand close to the sample surface, leading to bending of lattice planes

1
2
3
4
5 [27,28]. This effect strongly influences the intensity of the diffracted beams, because it leads
6
7 to a local variation of the excitation errors.
8

9
10 To estimate the influence of the specimen thickness uncertainty as well as the effect of strain,
11 CELFA evaluations of simulated images were carried out. Although the specimen thickness
12 in the experiments was estimated to be smaller than 70 nm from a comparison of the island
13 density in the image with the density obtained by plan-view TEM, images were simulated for
14 a specimen thickness between 10 and 200 nm. The COLC aimed at in the experiment was (0,
15 20, 1.5). To account for the effect of local tilt variation, which also have been reported in
16 literature [22,23], excitation conditions were varied corresponding to a COLC between (0, 20,
17 0) and (0, 20, 3). The local strain field was obtained by finite-element calculations. The finite
18 element (FE) models were generated according to the concentration profile (solid line in Fig.
19 3 for sample B). Using the column-approximation, the Howie-Whelan equations [29] were
20 solved with the fourth-order Runge-Kutta method and the complex amplitudes of diffracted
21 beams were calculated. The product of the amplitudes of the undiffracted and the 002 beam
22 corresponds to the amplitude A_{002} of the 002-Fourier coefficient of the image intensity for our
23 imaging conditions. Concentration profiles along the growth direction were evaluated from
24 the profiles of A_{002}^N according to the CELFA method. In analogy to the evaluation of the
25 experimental images, the simulated images were evaluated assuming a specimen thickness of
26 30 nm and a COLC of (0, 20, 1.5). [insert Figure 4 about here] As an example, Fig. 4 (left
27 axis) shows A_{002} simulated for 70 nm specimen thickness and a COLC of (0, 20, 1.25). The
28 variations of A_{002} in the regions below 0 nm and above 15 nm are caused by lattice plane
29 bending, which mainly affects the modulus of the undiffracted beam. The dashed line is the
30 fitted polynomial A_{002}^0 used to obtain normalized values A_{002}^N . Fig. 4 (right axis) also shows
31 the In-concentration evaluated from A_{002}^N , where a specimen thickness of 30 nm and a COLC
32 of (0, 20, 1.5) were assumed. For comparison, the solid line represents the true In-
33
34
35
36
37
38
39
40
41
42
43
44
45
46
47
48
49
50
51
52
53
54
55
56
57
58
59
60

1
2
3
4
5 concentration profile used as input for the simulation. Objective lens aberrations were not
6
7 taken into account, because we found that their influence can be neglected at the imaging
8
9 conditions applied [26]. [insert Figure 5 about here] To demonstrate that for the In-
10
11 concentration profile used here, Fig. 5 shows the original profile of A_{002} (same as in Fig. 4),
12
13 and profiles where the effect of lens aberrations were taken into account. Due to damping by
14
15 the transfer function of the objective lens, the original profile appears enlarged. All the
16
17 profiles computed for defocus values between -500 and +100 nm are very similar. Only the
18
19 parts below an abscissa of 0 nm and above 15 nm are affected slightly. This effect is due to
20
21 defocus-dependent delocalization of the undiffracted beam with respect to the 002 beam. Fig.
22
23 6 gives an overview of the results of our simulations. The maximum In-concentration
24
25 detected at the top of the central InGaAs layer is plotted versus the specimen thickness for the
26
27 different specimen orientations. [Insert figure 6 about here] One can clearly see that the effect
28
29 of specimen thickness uncertainty and strain fields yield measured maximum In-
30
31 concentrations that are slightly too large in most cases. Only for few certain combinations of
32
33 specimen thickness and specimen orientation, a decreased value of the measured maximum
34
35 concentration is encountered. The deviations are smallest for a COLC of (0, 20, 1.5) we
36
37 aimed at in the experiment. The lower straight solid line in Fig. 6 corresponds to the
38
39 maximum In-concentration measured in the case of sample B, clearly lying below the values
40
41 obtained by the simulation. Therefore, it seems not likely that these effects are responsible for
42
43 the deviation between the fitted segregation profile and the measured concentration profiles.
44
45
46
47
48
49
50
51 A third reason for the deviations, that seems more likely, is based on the presence of islands.
52
53 Here we assume that the amount of In atoms contained in the islands is missing in the wetting
54
55 layer. This could explain why the thickness of the wetting layers are approximately one ML
56
57 smaller than the nominal values. We assume that the islands are formed due to migration of
58
59 In-atoms from the wetting layer into the island. In addition, In atoms could also be provided
60

1
2
3
4
5 from the In-floating layer. This, however, seems unlikely, because a depletion of the In-
6
7 floating layer would result in an abrupt upper interface of the central InGaAs layers. In
8
9 contrast, the central InGaAs layers can be fitted with the same segregation efficiency as the
10
11 $\text{In}_{0.1}\text{Ga}_{0.9}\text{As}$ layers.
12

13
14 In layers grown by MBE, the 2D-3D transition occurs as soon as the amount of Indium in the
15
16 floating layer exceeds approximately 1.6 ML [7]. Fig. 7 shows the amount $x_s(n)$ of In-atoms
17
18 in the In-floating layer as obtained from equ. (1), plotted versus the number of MLs grown.
19
20 [Insert figure 7 about here] Fig. 7 shows that the amount of Indium in the floating layer was
21
22 less than 1 ML at the onset of the 2D-3D transition for both samples A and B. This finding is
23
24 in clear contrast to the behaviour of samples grown by MBE.
25
26

27
28 Our MOCVD samples reveal a segregation efficiency of $R=0.65\pm 0.05$ at a growth
29
30 temperature of 550 °C. [Insert figure 8 about here] Fig. 8 compares this value with
31
32 segregation efficiencies measured in MBE grown samples. It clearly reveals that the
33
34 segregation efficiency of our MOCVD samples is significantly smaller than those observed in
35
36 MBE grown samples at similar temperatures. The difference between MBE and MOCVD
37
38 grown samples can be explained by the different conditions and epitaxial processes at the
39
40 growth surface. It can be speculated that the flux of the H_2 carrier gas along the specimen
41
42 surface interferes with the formation of an In-floating layer which is only weakly bound to the
43
44 growth surface. A similar influence could be exerted by the large metal organic molecules
45
46 that are used to transport the Ga and In atoms onto the growth surface.
47
48
49
50
51
52
53
54
55
56
57
58
59
60

5. Conclusion

We measured In-concentration profiles of wetting layers in MOCVD grown InGaAs heterostructures buried in GaAs. The profiles clearly reveal that segregation of In takes place during growth. The fit of the concentration profiles with the Muraki model of segregation yield a segregation efficiency of $R=0.65\pm 0.05$ at the growth temperature of 550 °C. This value is considerably smaller than the efficiencies evaluated in MBE grown samples at similar temperature. The difference between MBE and MOCVD grown samples is tentatively explained by the flux of the carrier gas and the presence of large metal organic molecules at the growth surface in the case of MOCVD grown samples, which could hinder the formation of an indium floating layer that is only weakly bound to the growth surface. Indium concentrations measured on top of the wetting layers are smaller than expected from the Muraki model, and the thickness of the wetting layers is approximately 1 ML less than expected from the growth conditions. This deficiency of indium in the wetting layers is explained by a surface migration of In atoms from the wetting layer into the InGaAs quantum dots during growth. Applying the segregation model of Muraki, we estimate that the amount of In in the indium-floating layer is approximately 0.85 ML at the onset of the 2D-3D transition. This value is significantly smaller compared to MBE grown samples, where the growth mode transition occurs when the amount of Indium in the floating layer reaches 1.6 ML.

References

- [1] H. Drexler, D. Leonard, W. Hansen, J.P. Kottahaus, P.M. Petroff, Phys. Rev. Lett. **73**, (1994), p. 2252; D.L. Huffaker, G. Park, Z. Zou, O.B. Shchekin, and D.G. Deppe, Appl. Phys. Lett. **73** (1998), p. 2564.
- [2] Y. Arakawa, H. Sakaki: Appl. Phys. Lett. **40** (1982) 939.
- [3] J. Massies, F. Turco, A. Saletes and J.P. Contour, J. Cryst. Growth **80** (1987), p. 307-314.
- [4] S. Valeri, A. Di Bona, E. Engeli, S. Bordiga and A. Piccirillo, Thin Solid Films **197** (1991), p. 179-186.
- [5] J. M. Moison, C. Guille, F. Houzay, F. Barthe, M. Van Rompay, Phys. Rev. B **40**, no.9 (1989), 6149.
- [6] J.M. Gerard, Appl. Phys. Lett. **61** (1992), p. 2096-2098.
- [7] Toyoshima, T. Niwa, J. Yamzaki, A. Okamoto, Appl. Phys. Lett. **62**, (1993), p. 821.
- [8] K. Muraki, S. Fukatsu, Y. Shirakia and R. Ito, Appl. Phys. Lett. **61** (1992), p. 557.
- [9] A. Rosenauer, D. Gerthsen, D. Van Dyck, M. Arzberger, G. Böhm and G. Abstreiter, Phys. Rev. B **64** (2001), p. 245334.
- [10] K.R. Evans, R. Kaspi, J.E. Ehret, M. Skowronski, C.R. Jones, J. Vac. Sci. Technol. B **13** (1995), p. 1820-1823
- [11] J.M. Garcia, J.P. Silveira, F. Briones, Appl. Phys. Lett. **77**, (2000), p. 409.
- [12] S. Martini, A.A. Quivy, T.E. Lamas, M.J. da Silva, E.C.F. da Silva, J.R. Leite, J. Cryst. Growth **251** (2003), p. 101-105.
- [13] M. Larive, J. Nagle, J.P. Landesman, X. Marcadet, C. Mottet, and P. Bois, J. Vac. Sci. Technol. B **11** (1993), p. 1413.
- [14] Kaspi R, and Evans K R, Appl. Phys. Lett. **67** (1995), p. 819.
- [15] O. Dehaese, X. Wallart, and F. Mollot, Appl. Phys. Lett. **66** (1995), p. 52-54

- 1
2
3
4
5 [16] T. Walther, A.G. Culli, D.J. Norris, and M. Hopkinson, *Phys. Rev. Lett.* **86** (2001), p.
6
7 2381-2384.
8
9 [17] A.G. Cullis, D.J. Norris, T. Walther, M.A. Migiorato, M. Hopkinson, *Phys. Rev. B* **66**,
10
11 (2002), p. 81305(R).
12
13 [18] R. Arès, C.A. Tran, S.P. Watkins, *Appl. Phys. Lett.* **67**, (1995), p. 1576.
14
15 [19] A. Rosenauer, D. Gerthsen, *Ultramicroscopy* **76** (1999), p. 49.
16
17 [20] A. Rosenauer, *Transmission Electron Microscopy of Semiconductor Nanostructures: An*
18
19 *Analysis of Composition and Strain State*, Springer Tracts in Modern Physics 182,
20
21 Springer-Verlag Berlin Heidelberg, (2003).
22
23 [21] T. Walther, C.B. Boothroyd and C.J. Humphreys, *Inst. Phys. Conf. Ser.* **146** (1995), p.
24
25 11-16.
26
27 [22] T. Walther and C.J. Humphreys, *Inst. Phys. Conf. Ser.* **147** (1995), p. 103-106
28
29 [23] T. Walther, C.J. Humphreys, *J. Cryst. Growth* **197** (1999), p. 113-128.
30
31 [24] A. Rosenauer, M. Schowalter, F. Glas, D. Lamoen, to be published in *Phys. Rev. B*
32
33 (2005)
34
35 [25] F. Glas, *Inst. Phys. Conf. Ser.* **180** (2003), p. 191.
36
37 [26] A. Rosenauer, D. Gerthsen, D. Van Dyck, S. Van Aert and A.J. Den Dekker, *Inst. Phys.*
38
39 *Conf. Ser.* **180** (2003), p. 19.
40
41 [27] P. H. Jouneau, A. Tardot, G. Feuillet, H. Mariette and J. Cibert, *J. Appl. Phys.* **75** (1994),
42
43 p. 7310-7316.
44
45 [28] K. Tillmann, A. Thust, M. Lentzen, P. Swiatek, A. Förster, K. Urban, W. Laufs, D.
46
47 Gerthsen, T. Remmele and A. Rosenauer, *Phil. Mag. Lett.* **74** (1996), p. 309-315.
48
49
50 [29] Marc De Graef, *Introduction to Conventional Transmission Electron Microscopy*,
51
52 Cambridge University Press, 2003.
53
54 [30] J.- M. Gerard, *Appl. Phys. Lett.* **61** (1992), p. 2096.
55
56
57
58
59
60

1
2
3
4
5 [31] A. Rosenauer, W. Oberst, D. Litvinov, D. Gerthsen, A. Förster, R. Schmidt, Phys. Rev. B
6
7 **61** (2000), p. 8276-88.
8
9
10
11
12
13
14
15
16
17
18
19
20
21
22
23
24
25
26
27
28
29
30
31
32
33
34
35
36
37
38
39
40
41
42
43
44
45
46
47
48
49
50
51
52
53
54
55
56
57
58
59
60

For Peer Review Only

Figure Captions

Figure 1

[001] bright-field plan view TEM specimens images showing the contrast of quantum dots in samples A (left) and B (right).

Figure 2

Colour-coded maps of the In concentration in samples A and B, evaluated with the CELFA method.

Figure 3

In-concentration profiles obtained from samples A and B. The growth direction is from left to right. The error bars give the standard deviation encountered by averaging local concentration values along (002) lattice planes. The solid lines show the values of the concentration profile $x_b(n)$ as obtained from a fit of the experimental data with equ. (1). The dotted line corresponds to the In concentration $x_0(n)$ (see equ. (1)).

Figure 4

Left axis: Signed modulus A_{002} of the 002 Fourier component of the image intensity obtained for a specimen thickness of 70 nm and a COLC of (0,20,1.25). The solid line shows A_{002}^0 obtained by fitting a third-order polynomial to A_{002} within the regions $d < -5$ nm and $d > 15$ nm. Right axis: In-concentration profile obtained by evaluation of $A_{002}^N = A_{002}/A_{002}^0$ according to the CELFA method (line with circles) and profile of the true In-concentration (bold solid line) used as input for the simulation.

Figure 5

Profiles of the signed modulus A_{002} for a specimen thickness of 70 nm and a COLC of (0,20,1.25). The grey curve was computed without lens aberration. Aberrations were taken into account for the other curves, which were calculated for different values of the defocus. The imaging parameters used are: Spherical aberration constant 1.0 mm, beam semiconvergence 1 mrad, and defocus spread 10 nm.

Figure 6

Maximum In-concentration on top of the central InGaAs layer obtained by the CELFA evaluation of images simulated for different specimen thickness and specimen orientation (Center of Laue circle is (0, 20, L), where L is given in the legend). For the CELFA evaluation, a specimen thickness of 30 nm and a specimen orientation corresponding to a center of Laue circle (COLC) of (0, 20, 1.5) was assumed. The upper straight solid line shows the true In-concentration assumed for the simulation. The lower straight line shows the maximum In-concentration we obtained in the experiment.

Figure 7

Profiles of the amount $x_s(n)$ (s. equ. (1)) of Indium in the floating layer during growth, as obtained from the fit of equ. (1) to the concentration profiles measured. The upper graph corresponds to sample A and the lower one to sample B. (Note that in the literature (e.g. [7]), $x_s(n)$ is expressed in units of ML In. In their notation, 1 ML In corresponds to $x_s(n)=1$).

Figure 8

1
2
3
4
5 Comparison of the segregation efficiency of MOCVD samples investigated in this work with
6
7 values obtained for MBE grown samples in literature. The different values correspond to the
8
9 following references: Muraki [8], Moison [5], Larive [13], Gerard [30], Toyoshima [7], Kaspi
10
11 [14], Rosenauer 2001 [9] and Rosenauer 2000 [31].
12
13
14
15
16
17
18
19
20
21
22
23
24
25
26
27
28
29
30
31
32
33
34
35
36
37
38
39
40
41
42
43
44
45
46
47
48
49
50
51
52
53
54
55
56
57
58
59
60

For Peer Review Only

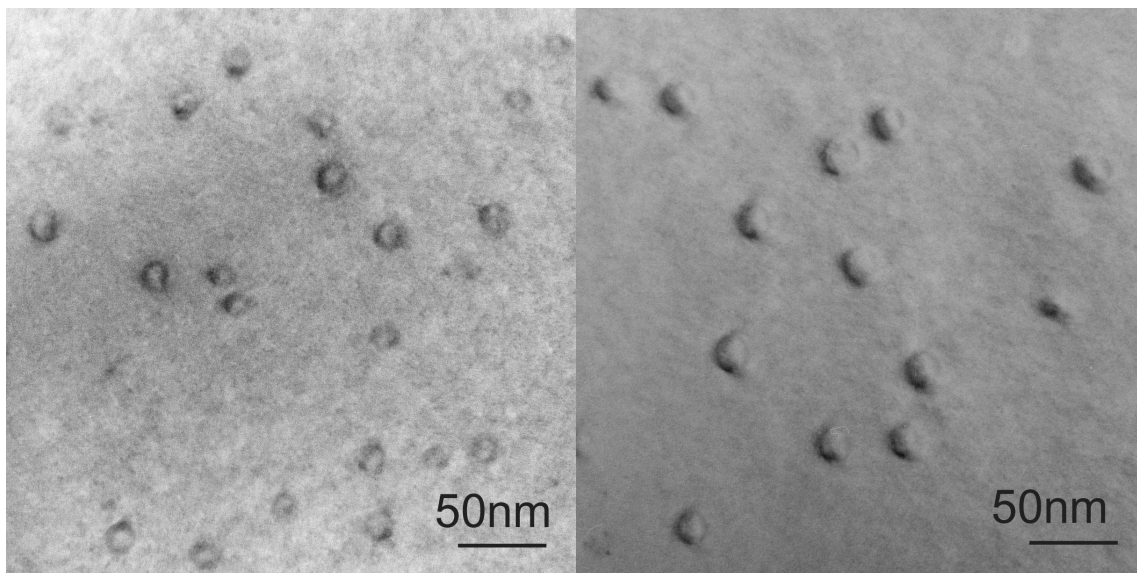


Figure 1

Review Only

1
2
3
4
5
6
7
8
9
10
11
12
13
14
15
16
17
18
19
20
21
22
23
24
25
26
27
28
29
30
31
32
33
34
35
36
37
38
39
40
41
42
43
44
45
46
47
48
49
50
51
52
53
54
55
56
57
58
59
60

1
2
3
4
5
6
7
8
9
10
11
12
13
14
15
16
17
18
19
20
21
22
23
24
25
26
27
28
29
30
31
32
33
34
35
36
37
38
39
40
41
42
43
44
45
46
47
48
49
50
51
52
53
54
55
56
57
58
59
60

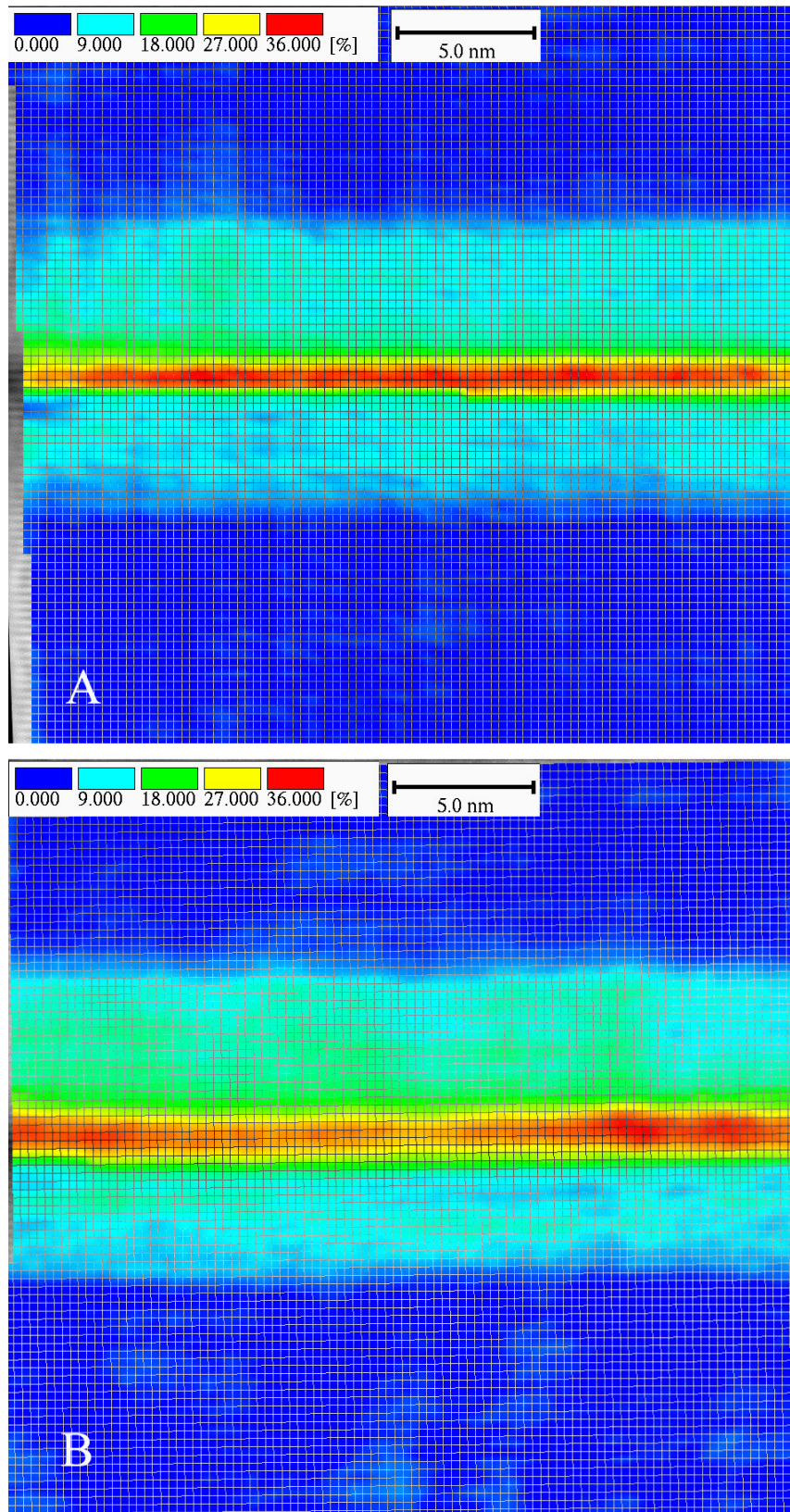


Figure 2

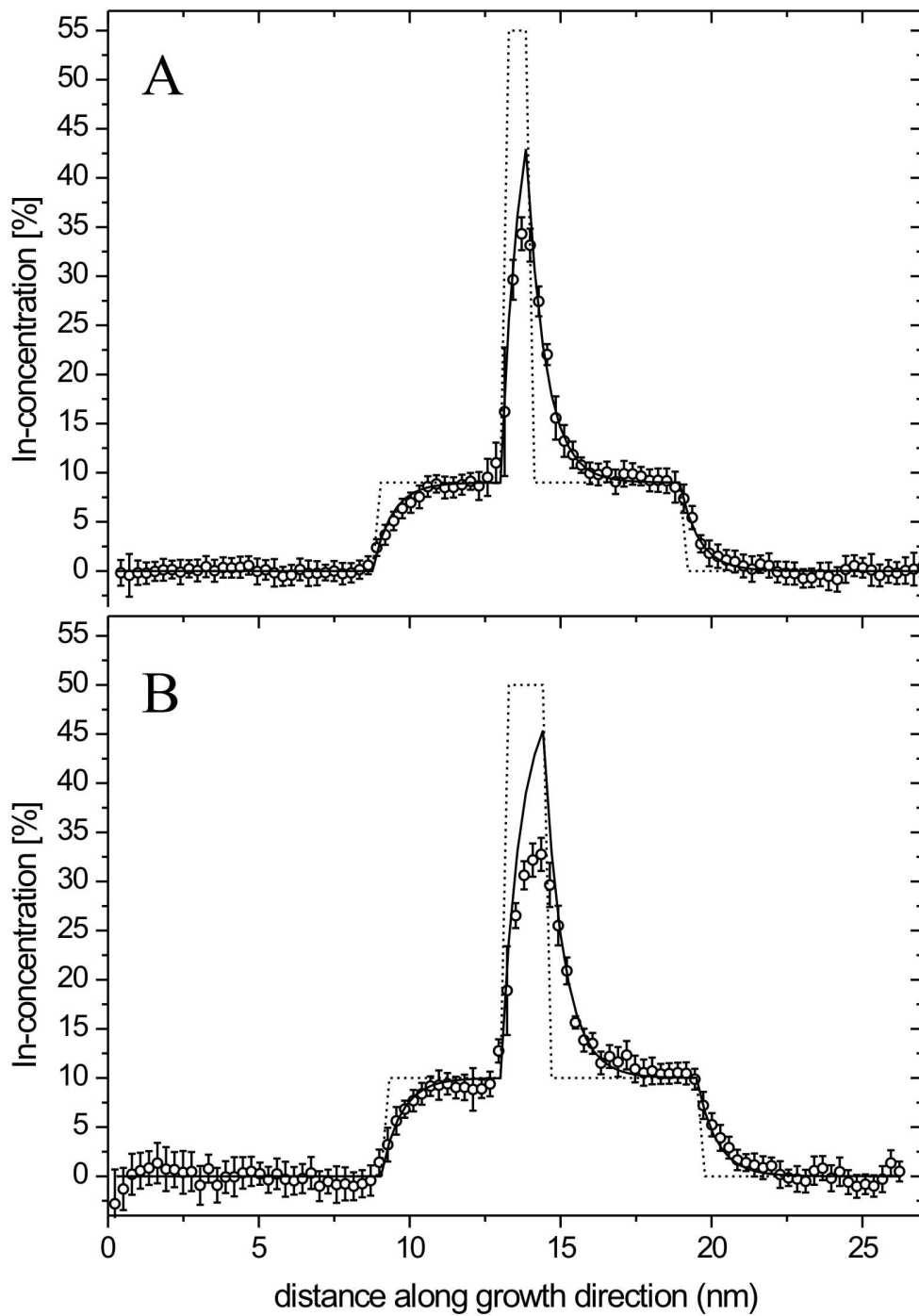


Figure 3

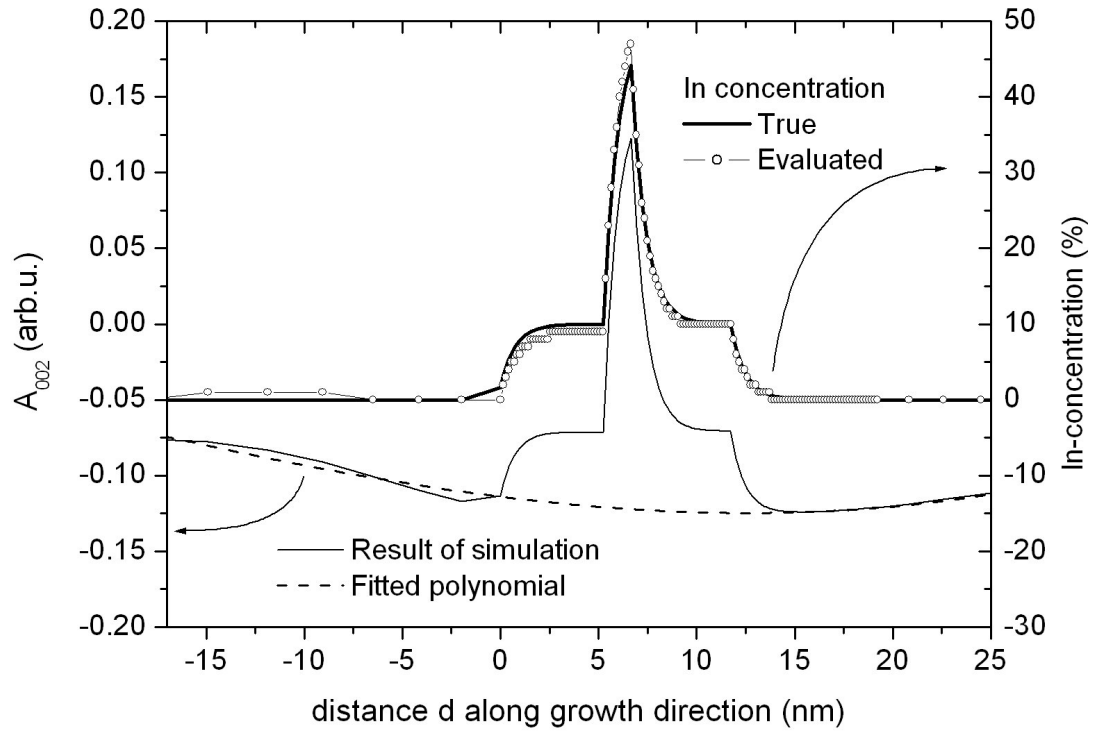


Figure 4

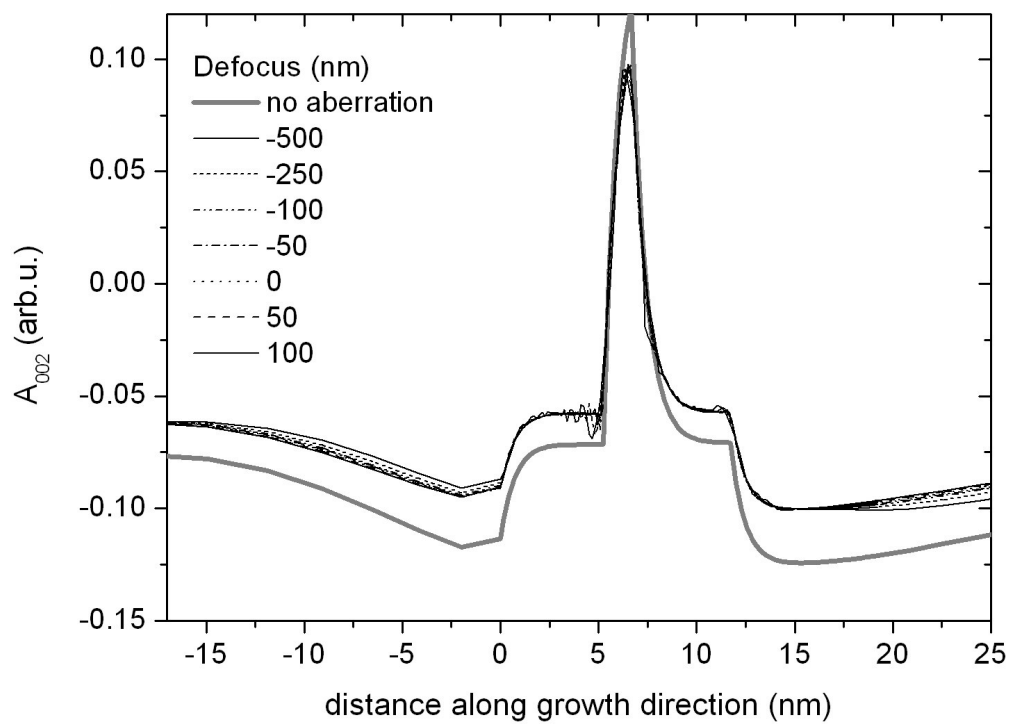


Figure 5

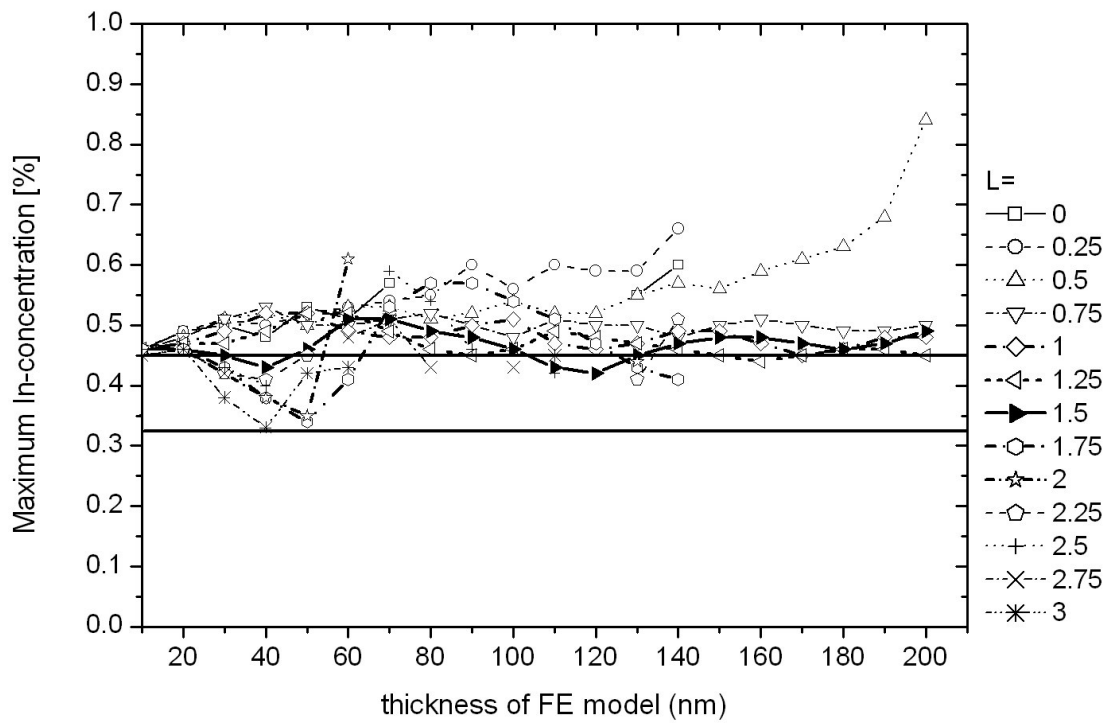


Figure 6

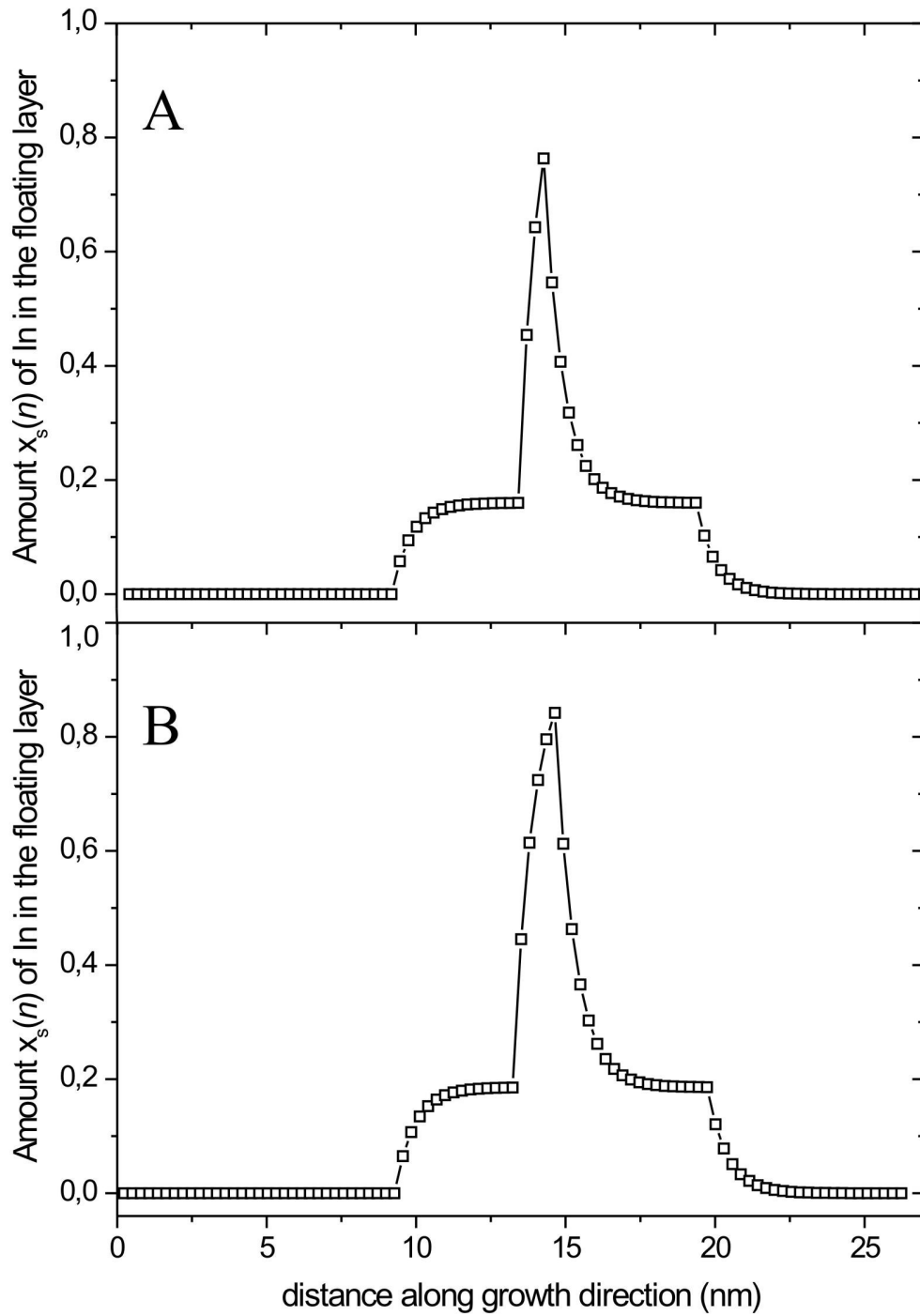


Figure 7

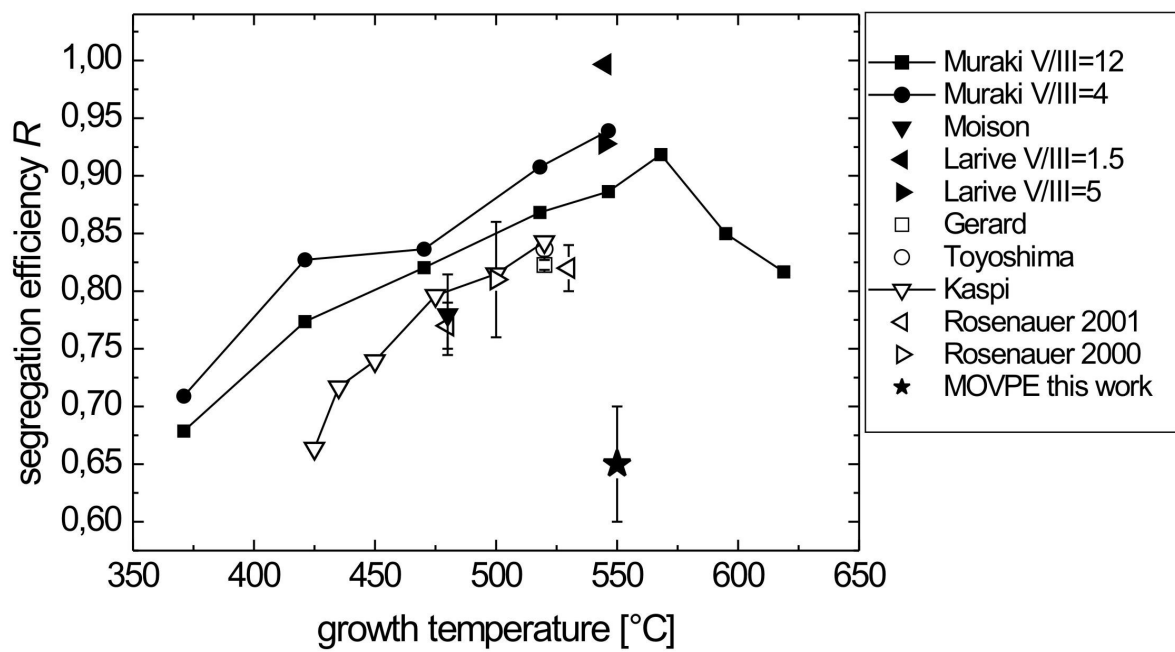


Figure 8

1
2
3
4
5 **Segregation in InGaAs/GaAs Stranski-Krastanow layers grown**
6
7
8 **by Metal Organic Vapour Phase Epitaxy**
9

10
11
12
13 E. PISCOPIELLO et al.
14
15

16
17
18 Complete list of the authors:
19

20 **Dr. Emanuela Piscopiello**
21

22 EMAT, University of Antwerp,
23 Groenenborgerlaan 171, B-2020 Antwerp, Belgium
24

25 Present address:
26

27 ENEA - C.R. Brindisi
28

29 Materials and New Technologies Unit
30

31 Composite and Nanostructured Materials Section
32

33 S.S. 7 - Km 714
34

35 72100 Brindisi (Italy)
36

37 Tel: +39 0831 201518
38

39 e-mail: emanuela.piscopiello@brindisi.enea.it
40

41 **Prof. Dr. Andreas Rosenauer**
42

43 IFP - University Bremen
44

45 Otto-Hahn-Allee 1, 28359 Bremen, GERMANY
46

47 Tel: ++49 (0)421 218.8197
48

49 Fax: ++49 (0)421 218.7381
50

51 Email: rosenauer@ifp.uni-bremen.de
52

53 **Dr. Adriana Passaseo**
54

55 National Nanotechnology Laboratory,
56

57 INFN-Unita` di Lecce c/o Dipartimento di Ingegneria
58

59 dell'Innovazione, Universita` di Lecce,
60

1
2
3
4
5 Via Arnesano, 73100 Lecce, Italy

6 Tel: +39 832 298206

7
8 Fax: +39 832 298238

9
10 Email: adriana.passaseo@unile.it
11
12

13
14 Eduardo Haroldo Montoya Rossi

15
16 Instituto Peruano de Energía Nuclear,

17
18 Av. Canada 1470, Lima 41, Perú

19
20 c/o Prof. Dr. Gustaaf Van Tendeloo, EMAT; Univ. of Antwerp
21
22

23
24
25 Prof. Dr. Gustaaf Van Tendeloo

26
27 EMAT, University of Antwerp,

28
29 Groenenborgerlaan 171, B-2020 Antwerp, Belgium

30
31 tel. : +32-3-2653262,

32
33 fax : +32-3-2653257,

34
35 Email : staf.vantendeloo@ua.ac.be
36
37
38
39
40
41
42
43
44
45
46
47
48
49
50
51
52
53
54
55
56
57
58
59
60

1
2
3
4
5 **Segregation in InGaAs/GaAs Stranski-Krastanow layers grown**
6
7
8 **by MOCVD**
9

10
11
12
13 E. PISCOPIELLO¹, A. ROSENAUER^{1,2}, A. PASSASEO³, E. H. MONTOYA ROSSI⁴, and
14
15 G. VAN TENDELOO¹.
16

17
18
19
20 1. EMAT, University of Antwerp, Groenenborgerlaan 171, B-2020 Antwerp, Belgium
21

22 2. IFP - University Bremen, Otto-Hahn-Allee 1, 28359 Bremen, GERMANY
23

24 3. NNL, University of Lecce, via Arnesano, 73100 Lecce, Italy
25

26 4. Instituto Peruano de Energía Nuclear, Av. Canada 1470, Lima 41, Perú .
27
28
29
30

31 **Abstract**
32

33
34 Using quantitative high resolution transmission electron microscopy we studied the chemical
35 morphology of wetting layers in InGaAs/GaAs quantum dot structures which were optimised
36 for applications to optical devices operating around 1.3 μm . The samples are grown by low-
37 pressure metal-organic chemical vapour deposition on GaAs substrates. Indium concentration
38 profiles of the wetting layers are evaluated with the composition evaluation by the lattice
39 fringe analysis method. The profiles reveal a clear signature of segregation. A fit of the
40 profiles with the Muraki model for segregation (K. Muraki et al., Appl. Phys. Lett. **61** (1992),
41 557) reveals a segregation efficiency of $R=0.65\pm 0.05$ at the growth temperature of 550 °C,
42 which is significantly lower than segregation efficiencies observed in samples grown by
43 molecular beam epitaxy at similar temperatures.
44
45
46
47
48
49
50
51
52
53
54
55
56
57
58
59
60

Keywords: HRTEM, image analysis, quantum dots, GaAs

1. Introduction

Low-dimensional semiconductor materials have become one of the most active research fields in solid state physics, chemistry and engineering. Quantum well (QW) and quantum-dot (QD) structures produced by epitaxial growth techniques (mainly molecular beam epitaxy (MBE) and metalorganic chemical vapour deposition (MOCVD)) are of considerable technological interest, since they are used as active components in devices, e.g. in high-electron-mobility transistors and optoelectronics [1]. Especially the InGaAs/GaAs material system is being studied intensively because of the possibility to form self-organized QDs by means of the Stranski-Krastanow growth mode under certain conditions. The development of QD lasers is expected to lead to increased quantum efficiency and to lower the threshold current density [2]. Properties of optoelectronic devices depend on the chemical morphology of the QWs or QDs forming the active region of a device. The growth of semiconductor nanostructures is governed by a complex and not fully understood interplay of surface and interface energies, formation of strain energy, elastic or plastic relaxation of strain energy, as well as by the kinetic growth processes such as adatom migration, interdiffusion and segregation.

Segregation is a known effect in MBE grown InGaAs/GaAs heterostructures [3,4] and leads to a strong enrichment of In on the growth surface compared to underlying completed mono layers (MLs). Moison et al. [5] attributed the effect to different chemical potentials of In and Ga atoms on the growth surface and suggested an exchange reaction of In and Ga in the topmost ("surface") layer and the underlying ("bulk") layer. The change of the free energy per atomic reaction was called the "segregation energy" E_S , and a value $E_S = 0.15$ eV was obtained [5] for InGaAs/GaAs at a growth temperature of 477 °C. Gerard [6] published a method to obtain the amount of In on the growth surface x_S by measuring a shift of the 2D-3D transition of InAs when grown on a predeposited layer of $\text{In}_{0.08}\text{Ga}_{0.92}\text{As}$. He found, that the amount of In on the surface of the predeposited layer with 8 % In was well described by the

1
2
3
4
5 segregation model of Moison [5] and obtained a segregation energy of $E_S = 0.17$ eV for a
6
7 growth temperature of 500 °C. For In-concentrations of the predeposited layer larger than 11
8
9 % he observed a strong deviation of x_S from the value predicted by the Moison model.
10
11 Toyoshima et al. [7] applied the method of Gerard to measure x_S for In-concentrations
12
13 between 15 % and 31 %. These authors found, that the amount of In x_S in the “In-floating
14
15 layer “ is well described by the phenomenological segregation model suggested by Muraki et
16
17 al. [8] also for nominal In-concentrations larger than 11 % where the Moison model failed.
18
19 Additionally, it was observed that the 2D-3D transition is correlated to the amount of In on
20
21 the growth surface and occurs when x_S reaches a value of more than 1.7 MLs. Rosenauer et
22
23 al. [9] measured In-concentration profiles of wetting layers in buried InAs/GaAs Stranski-
24
25 Krastanow structures by high-resolution transmission electron microscopy (HRTEM) and
26
27 found that the Muraki model [8] is in agreement with concentration profiles obtained. The
28
29 amount of In in the floating layer $x_S = 1.8$ MLs (1.5 MLs) was derived for growth temperatures
30
31 of 530 °C (480 °C) using a fit of the Muraki model to the experimental data. Evans et al. [10]
32
33 applied temperature-programmed desorption measurements and found that the steady-state In-
34
35 floating layer contains 1.3 ML (1.6 ML) In for a growth temperature of 480 °C (530 °C) and
36
37 that the surface-segregated In is liquid-like in character. Garcia et al. [11] found by in-situ
38
39 monitoring of stress acting on the GaAs substrate during the growth of InGaAs by MBE, that
40
41 the In-floating layer is not chemically bonded to the crystal surface. Further indication to the
42
43 mobile state of In atoms adsorbed in the In-floating layer has recently been given by RHEED
44
45 experiments carried out by Martini et al. [12]. The authors showed that the exponential
46
47 decrease of the RHEED oscillations observed at the onset of the InGaAs growth as well as the
48
49 increase of the signal during cap layer growth is caused by scattering of the electron beam by
50
51 mobile adatoms contained in the In-floating layer. Larive et al. [13] and Kaspi et al. [14]
52
53 observed an increase of the segregation with increasing growth temperature, which is in
54
55
56
57
58
59
60

1
2
3
4
5 contradiction to the Moison model [5]. Dehaese et al. [15] suggested a kinetic model
6
7 involving a two-energy level system which leads to the same segregation effect as the
8
9 Moison model for high growth temperatures larger than 500 °C, but additionally describes the
10
11 kinetic limitation of segregation at low temperature (400 °C). As shown by Gerard et al. [6],
12
13 this model is therefore also limited to In-concentrations below 11% for high growth
14
15 temperatures. Additionally, the exchange reaction of In and Ga between the surface and sub-
16
17 surface layer does not account for the liquid character of the In-atoms in the In-floating layer
18
19 evidenced recently [10,11,12], which limits x_S to values smaller or equal to 1 ML. Based on a
20
21 recent EFTEM study of Walther et al. [16], Cullis et al. [17] developed a segregation based
22
23 model for the critical thickness of the 2D-3D transition. In agreement with Toyoshima et al.
24
25 [7], the authors find that the 2D-3D transition occurs when the amount of In on the surface
26
27 exceeds a critical value. Applying the segregation model of Dehaese et al. [15] to InGaAs
28
29 layers with nominal In-concentrations of 25, 35 and 55 % at a growth temperature of 540 °C, a
30
31 critical value of $x_S=0.8-0.85$ MLs In was obtained.
32
33
34
35

36
37 During growth of a GaAs cap layer, the In-floating layer acts as a source for In atoms, leading
38
39 to a significant incorporation of In atoms into the cap layer. Thus, segregation leads to a
40
41 delayed incorporation of In atoms at the “lower” interface between the GaAs buffer and
42
43 InGaAs layer, and to an exponential decrease of the In-concentration within a GaAs cap layer
44
45 at the “upper” interface of the InGaAs layer.
46
47

48
49 Whereas segregation is intensively investigated for MBE grown structures, only little is
50
51 known about segregation during MOCVD growth. Evidence for segregation taking place in
52
53 atomic layer epitaxy using an MOCVD reactor was given by Arès et al. [18].
54

55
56 Here we present measurements of segregation efficiencies in MOCVD grown InGaAs/GaAs
57
58 using transmission electron microscopy (TEM) techniques. We evaluate In-concentration
59
60

1
2
3
4
5 profiles of the wetting layer (WL) of buried quantum dots and fit the results with the
6
7 segregation model of Muraki et al. [8].
8
9

10 11 12 **2. Experimental Set-Up**

13
14 The samples were grown in a horizontal low-pressure-MOCVD system (AIXTRON 200 AIX)
15
16 at 20 mbar with Trimethylgallium, Trimethylindium solution, and pure AsH₃ as source
17
18 materials; palladium purified H₂ with a flow rate of 7slm (standard litre per minute) was used
19
20 as a carrier gas. The growth was performed on (001) exactly oriented semi-insulating GaAs
21
22 substrates.
23
24

25
26 The investigated samples contain a 200 nm thick Si-doped GaAs buffer layer grown at a
27
28 temperature of 750°C, a 1- μ m Si-doped Al_{0.37}Ga_{0.63}As layer and a 80 nm GaAs layer,
29
30 followed by a 5 nm thick In_{0.10}Ga_{0.90}As layer, on top of which the deposition of the InGaAs
31
32 dots was carried out. The dots were covered with another 5 nm In_{0.10}Ga_{0.90}As and a 30 nm
33
34 thick GaAs cap layer. Two different samples were grown. In sample A, the thickness of the
35
36 InGaAs QD layer was 4 ML and the nominal In concentration $x_0=0.55$, whereas sample B
37
38 contains a 6 ML InGaAs QD layer with a nominal In concentration of $x_0=0.50$. During the
39
40 growth of the InGaAs layers, the growth temperature was fixed at 550 °C and the growth rate
41
42 at 1 ML/s. The AsH₃ partial pressure was kept at 1.4×10^{-1} mbar and 2.8×10^{-1} mbar for the
43
44 samples A and B, respectively. The In/Ga flow ratio was kept constant. During the capping
45
46 process the AsH₃ partial pressure was 5.7×10^{-1} mbar.
47
48
49

50
51 TEM samples were prepared by standard methods. Plan-view specimens were obtained by
52
53 grinding and polishing the substrate down to a thickness of about 20 μ m, followed by Ar ion
54
55 milling on the substrate side using an acceleration voltage of 4 kV and an incidence angle of
56
57 4°. Cross-section <001> and <110> TEM specimens were prepared by gluing two samples
58
59
60

1
2
3
4
5 face to face, cutting slices, dimple grinding and Ar ion milling. A JEOL 4000EX microscope
6
7 operating at 400kV with a Scherzer resolution of 0.17 nm was used.
8

9
10 Composition profiles of the wetting layers are obtained using the composition evaluation by
11 the lattice fringe analysis (CELFA) method [19,20]. (002) lattice fringe images are recorded
12 by tilting the specimen approximately 3°-5° around an axis perpendicular to both the electron
13 beam direction and the interface plane. The excitation condition aimed at corresponds to a
14 center of the Laue circle (COLC) of (0,20,1.5) (a COLC of (0,20,2) would correspond to a
15 strongly excited (004) reflection) and was adjusted by selected-area diffraction in a region
16 including the investigated area or lying close it. The (002) beam is aligned parallel to the
17 optical axis and the objective aperture is set around the (002) and (000) reflections. The
18 CELFA method uses the following analysis steps: first, the image is subdivided into square
19 shaped image unit cells with a size corresponding to the 002 lattice plane spacing. For each
20 image unit cell n , the (signed) modulus $A_{002}(n)$ of the 002 Fourier component of the image
21 intensity is obtained by Fourier analysis. To account for variations of specimen thickness and
22 tilts [21,22,23] within the image, we use the following approach: Bloch wave calculations of
23 the modulus $A_{002}(x)$ of the 002 Fourier component of the image intensity as a function of the
24 In-concentration x were carried out for different thicknesses and tilts of the specimen [20].
25 These calculations showed, that the normalized modulus $A^N_{002}(x) = A_{002}(x)/A_{002}(x=0)$ only
26 weakly depends on specimen thickness and tilt. Therefore, we normalize the experimental
27 values $A_{002}(n)$ with respect to the GaAs region according to $A^N_{002}(n) = A_{002}(n)/A^0_{002}(n)$. Since
28 specimen thickness and tilt may vary within the image, an appropriate value $A^0_{002}(n)$ has to be
29 used for each image unit cell n . By using parts of the image lying in the regions of the GaAs
30 substrate or cap layer, a 2-dimensional third-order polynomial $A^0_{002}(n)$ is fitted to the values
31 $A_{002}(n)$. The experimentally obtained normalized modulus is then compared with values
32 calculated with the Bloch wave method. The Bloch wave calculations are based on the
33
34
35
36
37
38
39
40
41
42
43
44
45
46
47
48
49
50
51
52
53
54
55
56
57
58
59
60

1
2
3
4
5 knowledge of the Fourier components of the crystal potential. We compute the Fourier
6
7 components of the crystal potential by density functional theory methods [24]. This is done to
8
9 avoid the isolated atom approximation frequently used in TEM simulations. Additionally, the
10
11 effect of static displacements [24,25] occurring in ternary semiconductor material is also
12
13 taken into account.
14
15

21 3. Experimental Results

22
23 Fig. 1 shows plan view images from both samples A and B; the shape and size of the QDs are
24
25 clearly comparable. The density of the QDs is $2.3 \times 10^{10} \text{ cm}^{-2}$ for A and $7 \times 10^9 \text{ cm}^{-2}$ for B.
26
27 [Insert figure 1 about here]
28
29

30 Fig. 2 reproduces colour-coded maps of the In distribution in the $\text{In}_{1-x}\text{Ga}_x\text{As}$ WL evaluated
31
32 with the CELFA method. Although care was taken during the exposure of the images to use
33
34 regions where QDs were not visible, both images reveal small fluctuations of the In-
35
36 concentration within the InGaAs QW. Since these fluctuation do not only occur in the central
37
38 layer with high In concentration but also in the areas with nominally 10 % In, they are most
39
40 probably caused by surface roughness or contamination caused by ion milling during the
41
42 TEM specimen preparation, or by locally varying specimen tilt. Another possible origin could
43
44 be the presence of small dots or parts of already formed dots, depending on how the sample
45
46 was cut during the TEM cross-sectional specimen preparation. [Insert figure 2 about here]
47
48
49

50
51 Fig. 2 clearly evidences that the In-concentration in A is a few percent larger than in B, in
52
53 agreement with the values of the nominal concentration ($x_{0,A}=0.55$ and $x_{0,B}=0.50$).
54

55 For the quantification of the segregation efficiency, concentration profiles along the [001]
56
57 growth direction were obtained by averaging the evaluated In concentration along (002)
58
59
60

lattice planes. The results are shown in Fig. 3 for both samples A and B (open circles). The figures reveal a clear signature of segregation. [Insert figure 3 about here]

The In concentration rapidly increases at the two lower interfaces, whereas it decreases exponentially at the two upper interfaces close to the cap layer. For the evaluation of the segregation efficiency the measured profiles were fitted by the Muraki model. To model different local nominal In-concentrations ($x_0=0$ in the GaAs buffer and cap layers, $x_0 \approx 0.1$ in the $\text{In}_{0.10}\text{Ga}_{0.90}\text{As}$ layer and $x_0 = 0.55(0.5)$ in the QD layer in sample A(B)), we used the following iterative formulation of the Muraki model:

$$\begin{aligned}
 I \quad & x_b(n) = x_s(n) + x_0(n) \\
 II \quad & x_s(n+1) = x_b(n)R \quad , \\
 III \quad & x_b(n) = x_b(n)(1-R)
 \end{aligned} \tag{1}$$

where n is the number of the ML, R is the segregation efficiency, $x_b(n)$ is the In concentration in the upper crystal ML after growth of the n -th ML, and $x_s(n)$ is the In concentration in the In floating layer after growth of the n -th ML. In the literature (e.g. see ref. [7]), the amount of In in the floating layer is given in units of ML In, where 1 ML In corresponds to $x_s(n) = 1$. In the following, we shall use both notations. Equ. (1) comprises the following steps:

- I. After growth of ML ($n-1$) all In atoms of the In floating layer are incorporated into the upper crystal layer (corresponding to $x_b(n)$) and also the In atoms from the In source are added (corresponding to $x_0(n)$).
- II. Then, a fraction R of the In atoms in the upper crystal layer segregate to the new floating layer (corresponding to $x_s(n+1)$).
- III. The amount of Indium in the upper ML is decreased by the fraction of In atoms that segregated into the floating layer.

1
2
3
4
5 In Equ. (1), the segregation efficiency R as well as the position and thickness of the layers
6
7 were used as fitting parameters. The result of the fit is also shown in Fig. 3. The solid line
8
9 corresponds to the fitted concentration profile $x_b(n)$, and the dotted line indicates $x_0(n)$.
10
11 Obviously, the measured concentration profiles can well be fitted by the Muraki model,
12
13 clearly revealing that segregation is also present in samples grown by the MOCVD process.
14
15 From the fit of the Muraki model to our concentration profiles we found that the segregation
16
17 efficiency is $R=0.65\pm 0.05$ for both samples A and B. For the thickness of the central layer we
18
19 obtained 3 ML for sample A and 5 ML for sample B, compared to the nominal values of 4
20
21 ML and 6 ML, respectively.
22
23
24
25
26
27

28 **4. Discussion**

29
30 Although the fitted concentration profiles are generally in a fair agreement with the
31
32 experimental profiles, significant deviations are observed in both samples at the top of the
33
34 central InGaAs layer where the In concentration is large. In sample A(B), the measured In
35
36 concentration is approximately $\Delta x = 7\%$ (10%) below the value of the fitted profile. This
37
38 deviation can be explained by different effects.
39
40

41 First, it can be an artefact of the measurement of the In-concentration by the CELFA method.
42
43 If the specimen thickness assumed for the CELFA evaluation (30 nm) is wrong, the
44
45 evaluation contains errors that increase with increasing In-concentration. As the CELFA
46
47 technique uses a simple imaging condition where the relevant information (the local
48
49 composition) is almost solely transferred by only one reflection (the chemically sensitive 002
50
51 reflection) centred on the optical axis, objective lens defocus related artefacts are negligible in
52
53 a wide defocus range between approximately -150 and 50 nm [26].
54
55
56

57 Second, the InGaAs layers are strained. In a thin TEM specimen, compressively strained
58
59 layers are able to expand close to the sample surface, leading to bending of lattice planes
60

1
2
3
4
5 [27,28]. This effect strongly influences the intensity of the diffracted beams, because it leads
6
7 to a local variation of the excitation errors.
8

9
10 To estimate the influence of the specimen thickness uncertainty as well as the effect of strain,
11 CELFA evaluations of simulated images were carried out. Although the specimen thickness
12 in the experiments was estimated to be smaller than 70 nm from a comparison of the island
13 density in the image with the density obtained by plan-view TEM, images were simulated for
14 a specimen thickness between 10 and 200 nm. The COLC aimed at in the experiment was (0,
15 20, 1.5). To account for the effect of local tilt variation, which also have been reported in
16 literature [22,23], excitation conditions were varied corresponding to a COLC between (0, 20,
17 0) and (0, 20, 3). The local strain field was obtained by finite-element calculations. The finite
18 element (FE) models were generated according to the concentration profile (solid line in Fig.
19 3 for sample B). Using the column-approximation, the Howie-Whelan equations [29] were
20 solved with the fourth-order Runge-Kutta method and the complex amplitudes of diffracted
21 beams were calculated. The product of the amplitudes of the undiffracted and the 002 beam
22 corresponds to the amplitude A_{002} of the 002-Fourier coefficient of the image intensity for our
23 imaging conditions. Concentration profiles along the growth direction were evaluated from
24 the profiles of A_{002}^N according to the CELFA method. In analogy to the evaluation of the
25 experimental images, the simulated images were evaluated assuming a specimen thickness of
26 30 nm and a COLC of (0, 20, 1.5). [insert Figure 4 about here] As an example, Fig. 4 (left
27 axis) shows A_{002} simulated for 70 nm specimen thickness and a COLC of (0, 20, 1.25). The
28 variations of A_{002} in the regions below 0 nm and above 15 nm are caused by lattice plane
29 bending, which mainly affects the modulus of the undiffracted beam. The dashed line is the
30 fitted polynomial A_{002}^0 used to obtain normalized values A_{002}^N . Fig. 4 (right axis) also shows
31 the In-concentration evaluated from A_{002}^N , where a specimen thickness of 30 nm and a COLC
32 of (0, 20, 1.5) were assumed. For comparison, the solid line represents the true In-

1
2
3
4
5 concentration profile used as input for the simulation. Objective lens aberrations were not
6
7 taken into account, because we found that their influence can be neglected at the imaging
8
9 conditions applied [26]. [insert Figure 5 about here] To demonstrate that for the In-
10
11 concentration profile used here, Fig. 5 shows the original profile of A_{002} (same as in Fig. 4),
12
13 and profiles where the effect of lens aberrations were taken into account. Due to damping by
14
15 the transfer function of the objective lens, the original profile appears enlarged. All the
16
17 profiles computed for defocus values between -500 and +100 nm are very similar. Only the
18
19 parts below an abscissa of 0 nm and above 15 nm are affected slightly. This effect is due to
20
21 defocus-dependent delocalization of the undiffracted beam with respect to the 002 beam. Fig.
22
23 6 gives an overview of the results of our simulations. The maximum In-concentration
24
25 detected at the top of the central InGaAs layer is plotted versus the specimen thickness for the
26
27 different specimen orientations. [Insert figure 6 about here] One can clearly see that the effect
28
29 of specimen thickness uncertainty and strain fields yield measured maximum In-
30
31 concentrations that are slightly too large in most cases. Only for few certain combinations of
32
33 specimen thickness and specimen orientation, a decreased value of the measured maximum
34
35 In-concentrations that are slightly too large in most cases. Only for few certain combinations of
36
37 specimen thickness and specimen orientation, a decreased value of the measured maximum
38
39 concentration is encountered. The deviations are smallest for a COLC of (0, 20, 1.5) we
40
41 aimed at in the experiment. The lower straight solid line in Fig. 6 corresponds to the
42
43 maximum In-concentration measured in the case of sample B, clearly lying below the values
44
45 obtained by the simulation. Therefore, it seems not likely that these effects are responsible for
46
47 the deviation between the fitted segregation profile and the measured concentration profiles.
48
49

50
51 A third reason for the deviations, that seems more likely, is based on the presence of islands.
52
53 Here we assume that the amount of In atoms contained in the islands is missing in the wetting
54
55 layer. This could explain why the thickness of the wetting layers are approximately one ML
56
57 smaller than the nominal values. We assume that the islands are formed due to migration of
58
59 In-atoms from the wetting layer into the island. In addition, In atoms could also be provided
60

1
2
3
4
5 from the In-floating layer. This, however, seems unlikely, because a depletion of the In-
6
7 floating layer would result in an abrupt upper interface of the central InGaAs layers. In
8
9 contrast, the central InGaAs layers can be fitted with the same segregation efficiency as the
10
11 $\text{In}_{0.1}\text{Ga}_{0.9}\text{As}$ layers.
12

13
14 In layers grown by MBE, the 2D-3D transition occurs as soon as the amount of Indium in the
15
16 floating layer exceeds approximately 1.6 ML [7]. Fig. 7 shows the amount $x_s(n)$ of In-atoms
17
18 in the In-floating layer as obtained from equ. (1), plotted versus the number of MLs grown.
19
20 [Insert figure 7 about here] Fig. 7 shows that the amount of Indium in the floating layer was
21
22 less than 1 ML at the onset of the 2D-3D transition for both samples A and B. This finding is
23
24 in clear contrast to the behaviour of samples grown by MBE.
25
26

27
28 Our MOCVD samples reveal a segregation efficiency of $R=0.65\pm 0.05$ at a growth
29
30 temperature of 550 °C. [Insert figure 8 about here] Fig. 8 compares this value with
31
32 segregation efficiencies measured in MBE grown samples. It clearly reveals that the
33
34 segregation efficiency of our MOCVD samples is significantly smaller than those observed in
35
36 MBE grown samples at similar temperatures. The difference between MBE and MOCVD
37
38 grown samples can be explained by the different conditions and epitaxial processes at the
39
40 growth surface. It can be speculated that the flux of the H_2 carrier gas along the specimen
41
42 surface interferes with the formation of an In-floating layer which is only weakly bound to the
43
44 growth surface. A similar influence could be exerted by the large metal organic molecules
45
46 that are used to transport the Ga and In atoms onto the growth surface.
47
48
49
50
51
52
53
54
55
56
57
58
59
60

5. Conclusion

We measured In-concentration profiles of wetting layers in MOCVD grown InGaAs heterostructures buried in GaAs. The profiles clearly reveal that segregation of In takes place during growth. The fit of the concentration profiles with the Muraki model of segregation yield a segregation efficiency of $R=0.65\pm 0.05$ at the growth temperature of 550 °C. This value is considerably smaller than the efficiencies evaluated in MBE grown samples at similar temperature. The difference between MBE and MOCVD grown samples is tentatively explained by the flux of the carrier gas and the presence of large metal organic molecules at the growth surface in the case of MOCVD grown samples, which could hinder the formation of an indium floating layer that is only weakly bound to the growth surface. Indium concentrations measured on top of the wetting layers are smaller than expected from the Muraki model, and the thickness of the wetting layers is approximately 1 ML less than expected from the growth conditions. This deficiency of indium in the wetting layers is explained by a surface migration of In atoms from the wetting layer into the InGaAs quantum dots during growth. Applying the segregation model of Muraki, we estimate that the amount of In in the indium-floating layer is approximately 0.85 ML at the onset of the 2D-3D transition. This value is significantly smaller compared to MBE grown samples, where the growth mode transition occurs when the amount of Indium in the floating layer reaches 1.6 ML.

References

- [1] H. Drexler, D. Leonard, W. Hansen, J.P. Kottahaus, P.M. Petroff, Phys. Rev. Lett. **73**, (1994), p. 2252; D.L. Huffaker, G. Park, Z. Zou, O.B. Shchekin, and D.G. Deppe, Appl. Phys. Lett. **73** (1998), p. 2564.
- [2] Y. Arakawa, H. Sakaki: Appl. Phys. Lett. **40** (1982) 939.
- [3] J. Massies, F. Turco, A. Saletes and J.P. Contour, J. Cryst. Growth **80** (1987), p. 307-314.
- [4] S. Valeri, A. Di Bona, E. Engeli, S. Bordiga and A. Piccirillo, Thin Solid Films **197** (1991), p. 179-186.
- [5] J. M. Moison, C. Guille, F. Houzay, F. Barthe, M. Van Rompay, Phys. Rev. B **40**, no.9 (1989), 6149.
- [6] J.M. Gerard, Appl. Phys. Lett. **61** (1992), p. 2096-2098.
- [7] Toyoshima, T. Niwa, J. Yamzaki, A. Okamoto, Appl. Phys. Lett. **62**, (1993), p. 821.
- [8] K. Muraki, S. Fukatsu, Y. Shirakia and R. Ito, Appl. Phys. Lett. **61** (1992), p. 557.
- [9] A. Rosenauer, D. Gerthsen, D. Van Dyck, M. Arzberger, G. Böhm and G. Abstreiter, Phys. Rev. B **64** (2001), p. 245334.
- [10] K.R. Evans, R. Kaspi, J.E. Ehret, M. Skowronski, C.R. Jones, J. Vac. Sci. Technol. B **13** (1995), p. 1820-1823
- [11] J.M. Garcia, J.P. Silveira, F. Briones, Appl. Phys. Lett. **77**, (2000), p. 409.
- [12] S. Martini, A.A. Quivy, T.E. Lamas, M.J. da Silva, E.C.F. da Silva, J.R. Leite, J. Cryst. Growth **251** (2003), p. 101-105.
- [13] M. Larive, J. Nagle, J.P. Landesman, X. Marcadet, C. Mottet, and P. Bois, J. Vac. Sci. Technol. B **11** (1993), p. 1413.
- [14] Kaspi R, and Evans K R, Appl. Phys. Lett. **67** (1995), p. 819.
- [15] O. Dehaese, X. Wallart, and F. Mollot, Appl. Phys. Lett. **66** (1995), p. 52-54

- 1
2
3
4
5 [16] T. Walther, A.G. Culli, D.J. Norris, and M. Hopkinson, Phys. Rev. Lett. **86** (2001), p.
6
7 2381-2384.
8
9
10 [17] A.G. Cullis, D.J. Norris, T. Walther, M.A. Migiorato, M. Hopkinson, Phys. Rev. B **66**,
11
12 (2002), p. 81305(R).
13
14 [18] R. Arès, C.A. Tran, S.P. Watkins, Appl. Phys. Lett. **67**, (1995), p. 1576.
15
16 [19] A. Rosenauer, D. Gerthsen, Ultramicroscopy **76** (1999), p. 49.
17
18 [20] A. Rosenauer, *Transmission Electron Microscopy of Semiconductor Nanostructures: An*
19
20 *Analysis of Composition and Strain State*, Springer Tracts in Modern Physics 182,
21
22 Springer-Verlag Berlin Heidelberg, (2003).
23
24 [21] T. Walther, C.B. Boothroyd and C.J. Humphreys, Inst. Phys. Conf. Ser. **146** (1995), p.
25
26 11-16.
27
28 [22] T. Walther and C.J. Humphreys, Inst. Phys. Conf. Ser. **147** (1995), p. 103-106
29
30 [23] T. Walther, C.J. Humphreys, J. Cryst. Growth **197** (1999), p. 113-128.
31
32 [24] A. Rosenauer, M. Schowalter, F. Glas, D. Lamoen, to be published in Phys. Rev. B
33
34 (2005)
35
36 [25] F. Glas, Inst. Phys. Conf. Ser. **180** (2003), p. 191.
37
38 [26] A. Rosenauer, D. Gerthsen, D. Van Dyck, S. Van Aert and A.J. Den Dekker, Inst. Phys.
39
40 Conf. Ser. **180** (2003), p. 19.
41
42 [27] P. H. Jouneau, A. Tardot, G. Feuillet, H. Mariette and J. Cibert, J. Appl. Phys. **75** (1994),
43
44 p. 7310-7316.
45
46 [28] K. Tillmann, A. Thust, M. Lentzen, P. Swiatek, A. Förster, K. Urban, W. Laufs, D.
47
48 Gerthsen, T. Remmele and A. Rosenauer, Phil. Mag. Lett. **74** (1996), p. 309-315.
49
50 [29] Marc De Graef, *Introduction to Conventional Transmission Electron Microscopy*,
51
52 Cambridge University Press, 2003.
53
54 [30] J.- M. Gerard, Appl. Phys. Lett. **61** (1992), p. 2096.
55
56
57
58
59
60

[31] A. Rosenauer, W. Oberst, D. Litvinov, D. Gerthsen, A. Förster, R. Schmidt, Phys. Rev. B
61 (2000), p. 8276-88.

For Peer Review Only

1
2
3
4
5
6
7
8
9
10
11
12
13
14
15
16
17
18
19
20
21
22
23
24
25
26
27
28
29
30
31
32
33
34
35
36
37
38
39
40
41
42
43
44
45
46
47
48
49
50
51
52
53
54
55
56
57
58
59
60

Figure Captions

Figure 1

[001] bright-field plan view TEM specimens images showing the contrast of quantum dots in samples A (left) and B (right).

Figure 2

Colour-coded maps of the In concentration in samples A and B, evaluated with the CELFA method.

Figure 3

In-concentration profiles obtained from samples A and B. The growth direction is from left to right. The error bars give the standard deviation encountered by averaging local concentration values along (002) lattice planes. The solid lines show the values of the concentration profile $x_b(n)$ as obtained from a fit of the experimental data with equ. (1). The dotted line corresponds to the In concentration $x_0(n)$ (see equ. (1)).

Figure 4

Left axis: Signed modulus A_{002} of the 002 Fourier component of the image intensity obtained for a specimen thickness of 70 nm and a COLC of (0,20,1.25). The solid line shows A_{002}^0 , obtained by fitting a third-order polynomial to A_{002} within the regions $d < -5$ nm and $d > 15$ nm. Right axis: In-concentration profile obtained by evaluation of $A_{002}^N = A_{002}/A_{002}^0$ according to the CELFA method (line with circles) and profile of the true In-concentration (bold solid line) used as input for the simulation.

Figure 5

Profiles of the signed modulus A_{002} for a specimen thickness of 70 nm and a COLC of (0,20,1.25). The grey curve was computed without lens aberration. Aberrations were taken into account for the other curves, which were calculated for different values of the defocus. The imaging parameters used are: Spherical aberration constant 1.0 mm, beam semiconvergence 1 mrad, and defocus spread 10 nm.

Figure 6

Maximum In-concentration on top of the central InGaAs layer obtained by the CELFA evaluation of images simulated for different specimen thickness and specimen orientation (Center of Laue circle is (0, 20, L), where L is given in the legend). For the CELFA evaluation, a specimen thickness of 30 nm and a specimen orientation corresponding to a center of Laue circle (COLC) of (0, 20, 1.5) was assumed. The upper straight solid line shows the true In-concentration assumed for the simulation. The lower straight line shows the maximum In-concentration we obtained in the experiment.

Figure 7

Profiles of the amount $x_s(n)$ (s. equ. (1)) of Indium in the floating layer during growth, as obtained from the fit of equ. (1) to the concentration profiles measured. The upper graph corresponds to sample A and the lower one to sample B. (Note that in the literature (e.g. [7]), $x_s(n)$ is expressed in units of ML In. In their notation, 1 ML In corresponds to $x_s(n)=1$).

Figure 8

1
2
3
4
5 Comparison of the segregation efficiency of MOCVD samples investigated in this work with
6
7 values obtained for MBE grown samples in literature. The different values correspond to the
8
9 following references: Muraki [8], Moison [5], Larive [13], Gerard [30], Toyoshima [7], Kaspi
10
11 [14], Rosenauer 2001 [9] and Rosenauer 2000 [31].
12
13
14
15
16
17
18
19
20
21
22
23
24
25
26
27
28
29
30
31
32
33
34
35
36
37
38
39
40
41
42
43
44
45
46
47
48
49
50
51
52
53
54
55
56
57
58
59
60

For Peer Review Only

1
2
3
4
5
6
7
8
9
10
11
12
13
14
15
16
17
18
19
20
21
22
23
24
25
26
27
28
29
30
31
32
33
34
35
36
37
38
39
40
41
42
43
44
45
46
47
48
49
50
51
52
53
54
55
56
57
58
59
60

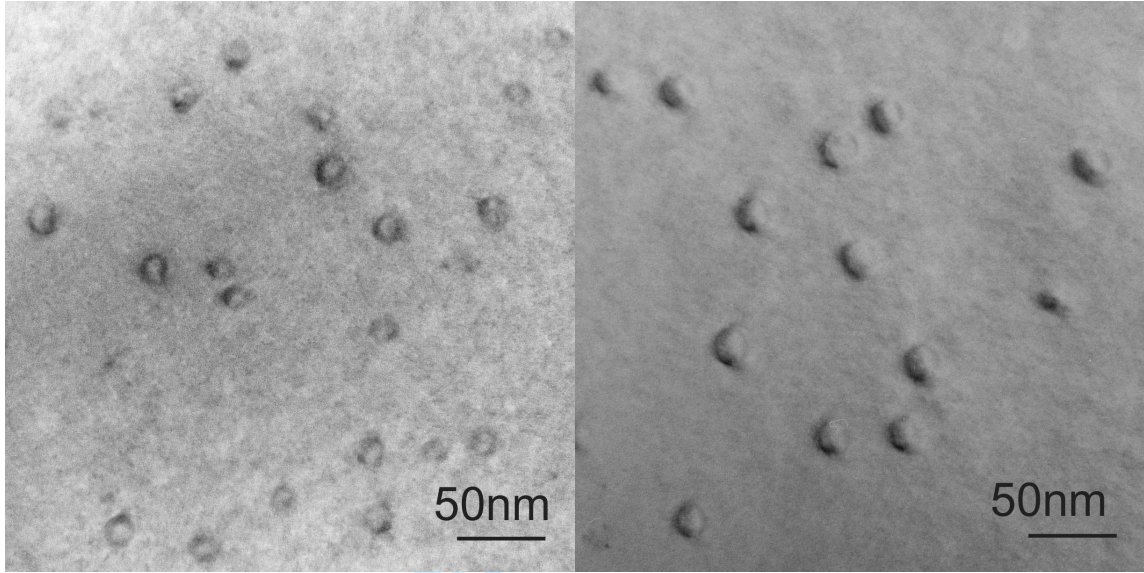


Figure 1

1
2
3
4
5
6
7
8
9
10
11
12
13
14
15
16
17
18
19
20
21
22
23
24
25
26
27
28
29
30
31
32
33
34
35
36
37
38
39
40
41
42
43
44
45
46
47
48
49
50
51
52
53
54
55
56
57
58
59
60

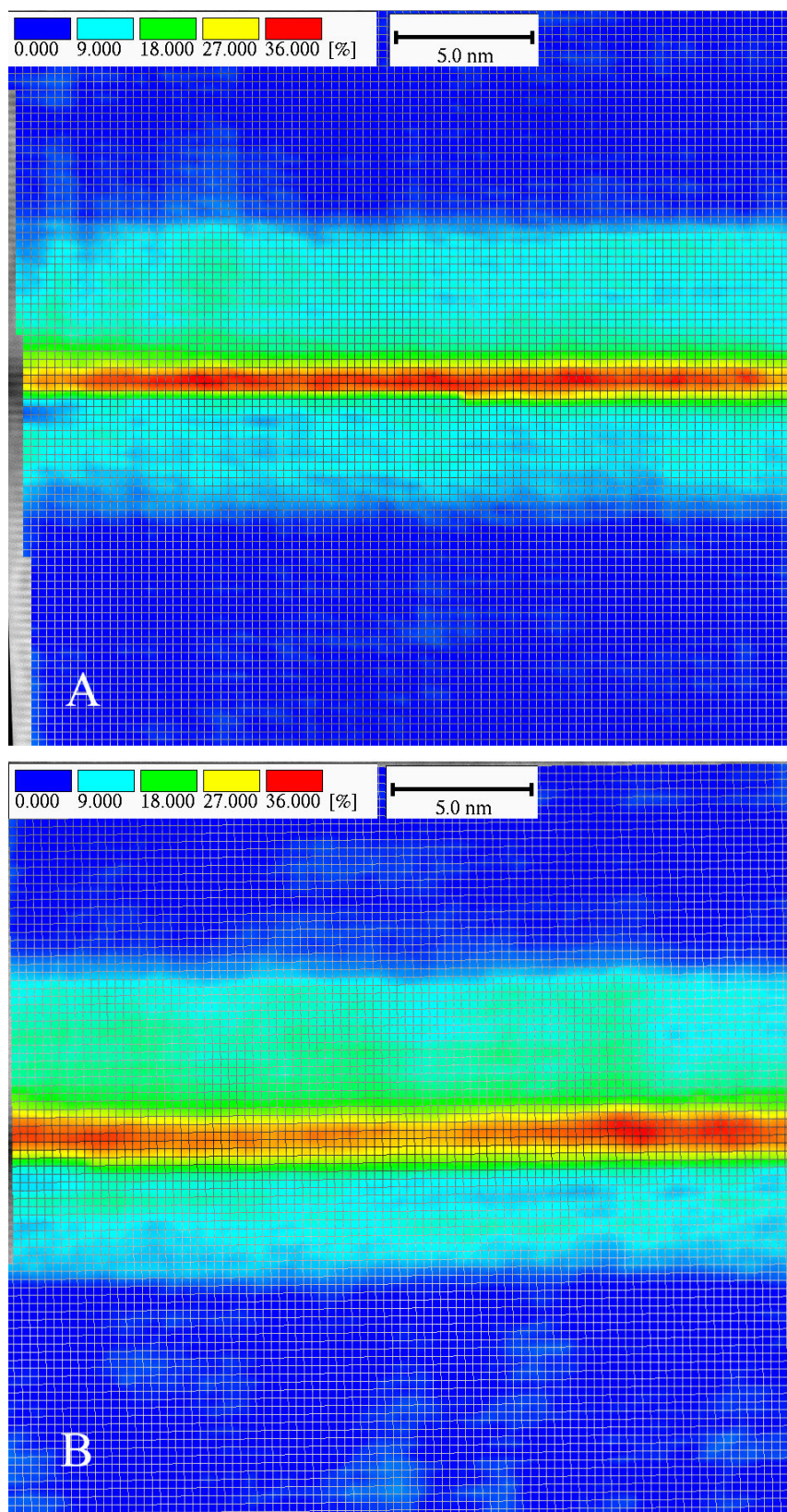


Figure 2

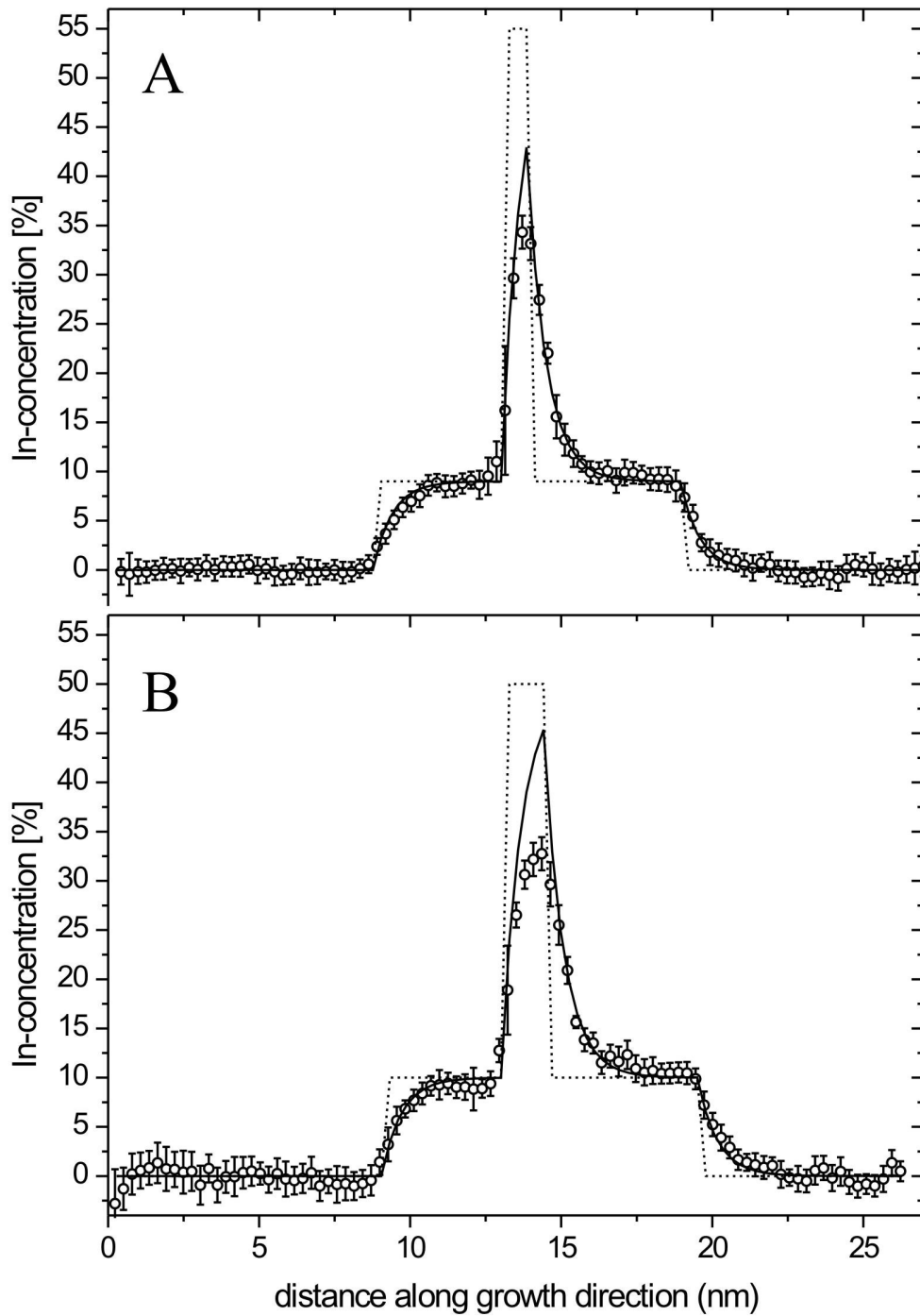


Figure 3

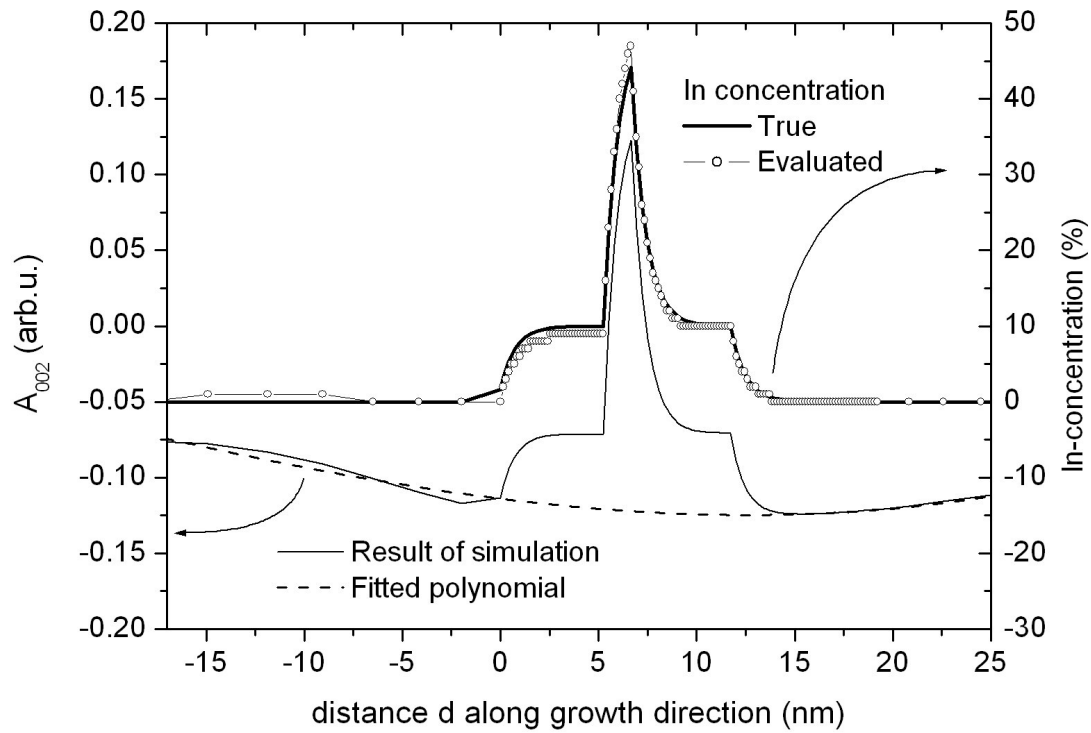


Figure 4

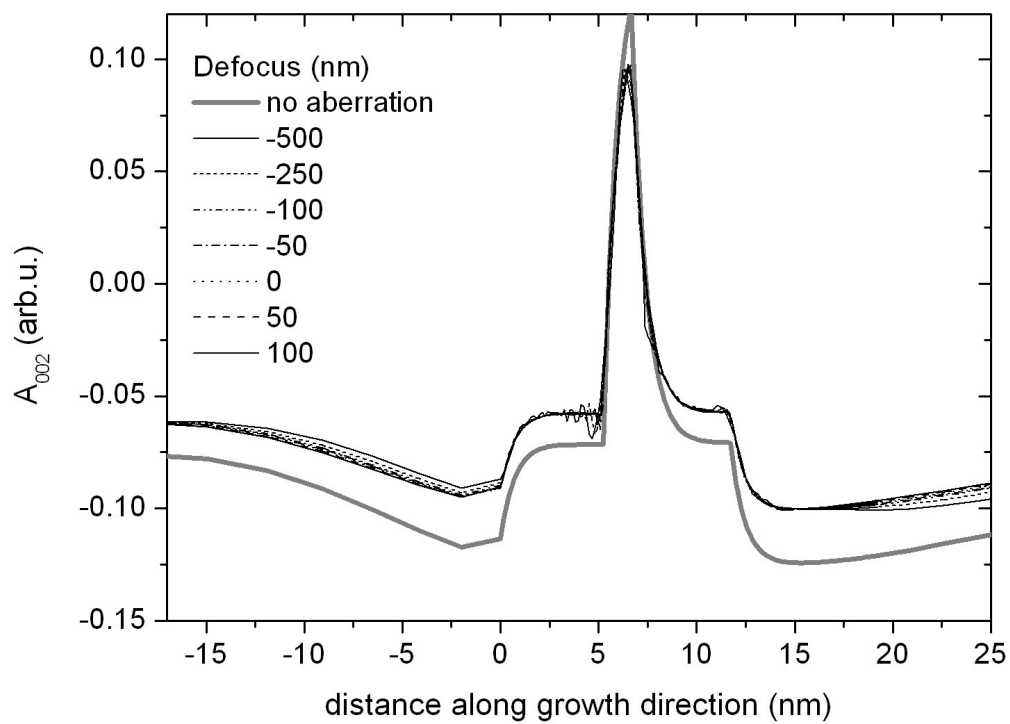


Figure 5

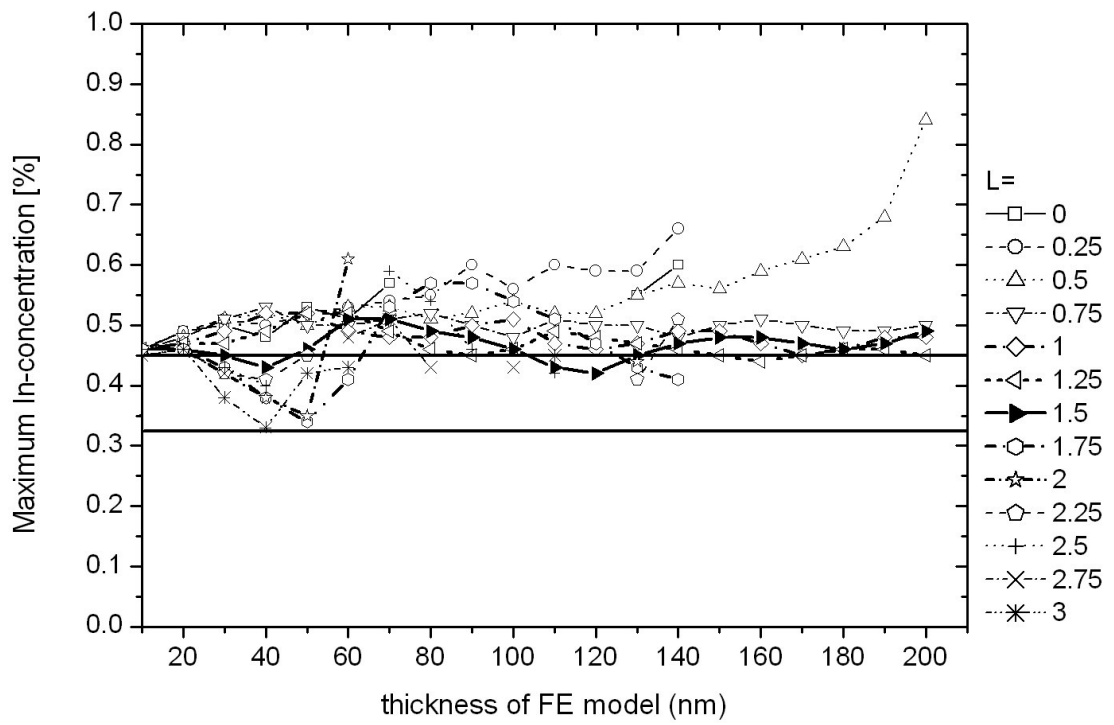


Figure 6

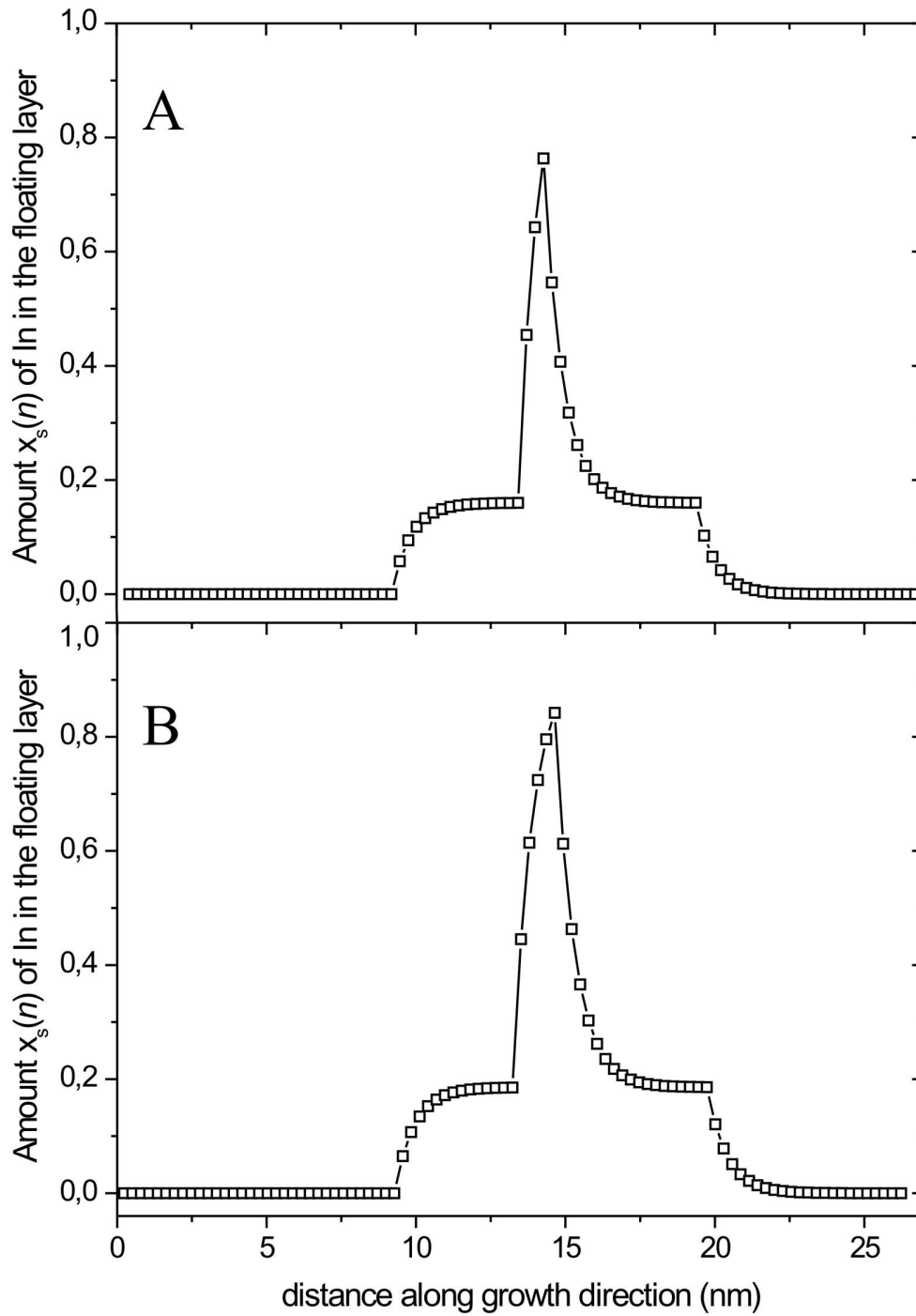


Figure 7

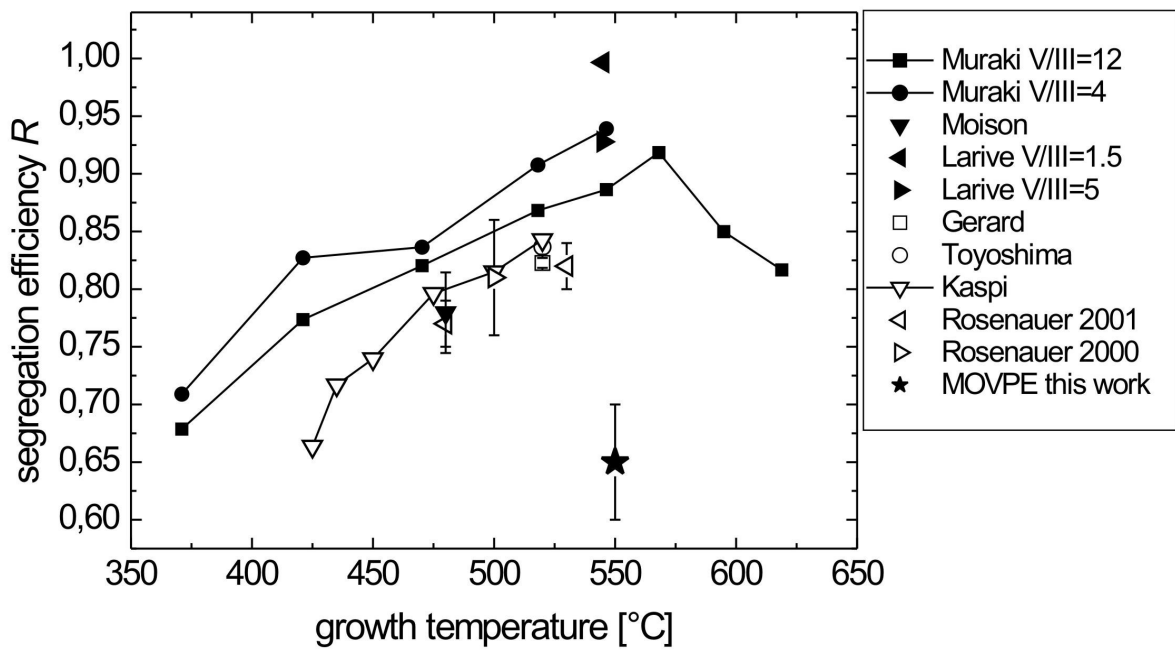


Figure 8